Geophysical Journal International

Geophys. J. Int. (2020) **220,** 522–540 doi: 10.1093/gji/ggz424
Advance Access publication 2019 October 07
Geodynamics and Tectonics

Regional crustal and lithospheric thickness model for Alaska, the Chukchi shelf, and the inner and outer bering shelves

Montserrat Torne,[1] Ivone Jiménez–Munt,[1] Jaume Vergés,[1] Manel Fernàndez,[1] Alberto Carballo[1,2] and Margarete Jadamec[3,4]

[1] *Group of Dynamics of the Lithosphere, Institute of Earth Sciences Jaume Almera, ICTJA–CSIC, Barcelona, E-08028, Spain. E-mail: montserrat.torne@ictja.csic.es*
[2] *Department of Earth and Atmospheric Sciences, University of Houston, Houston, TX-77004, TX, USA*
[3] *Department of Geology, University at Buffalo, The State University of New York, Buffalo, NY, NY-14260, USA*
[4] *Computational and Data-Enabled Science and Engineering Program, University at Buffalo, The State University of New York, Buffalo, NY, USA*

Accepted 2019 October 3. Received 2019 August 9; in original form 2019 April 13

SUMMARY

This study presents for the first time an integrated image of the crust and lithospheric mantle of Alaska and its adjacent western shelves of the Chukchi and Bering seas based on joint modelling of potential field data constrained by thermal analysis and seismic data. We also perform 3-D forward modelling and inversion of Bouguer anomalies to analyse density heterogeneities at the crustal level. The obtained crustal model shows northwest-directed long wavelength thickening (32–36 km), with additional localized trends of thicker crust in the Brooks Range (40 km) and in the Alaska and St Elias ranges (50 km). Offshore, 28–30-km-thick crust is predicted near the Bearing slope break and 36–38 km in the northern Chukchi Shelf. In interior Alaska, the crustal thickness changes abruptly across the Denali fault, from 34–36 to the north to above 30 km to the south. This sharp crustal thickness gradient agrees with the presence of a crustal tectonic buttress guiding block motion west and south towards the subduction zone. The average crustal density is 2810 $kg\,m^{-3}$. The denser crust, up to 2910 $kg\,m^{-3}$, is found south of the Denali Fault likely related to the oceanic nature of the Wrangellia Composite Terrane rocks. Offshore, less dense crust ($<2800\ kg\,m^{-3}$) is found along the sedimentary basins of the Chukchi and Beaufort shelves. At LAB levels, there is a regional SE–NW trend that coincides with the current Pacific Plate motion, with a lithospheric root underneath the Brooks Range, Northern Slope, and Chuckchi Sea, that may correspond to a relic of the Chukotka-Artic Alaska microplate. The obtained lithospheric root (above 180 km) agrees with the presence of a boundary of cold, strong lithosphere that deflects the strain towards the South. South of the Denali Fault the LAB topography is quite complex. East of 150°W, below Wrangellia and the eastern side of Chugach terranes, the LAB is much shallower than it is west of this meridian. The NW trending limit separating thinner lithosphere in the east and thicker in the west agrees with the two-tiered slab shape of the subducting Pacific Plate.

Key words: Gravity anomalies and Earth structure; Arctic region; Continental margins: convergent; Crustal structure; Dynamics: gravity and tectonics.

1 INTRODUCTION

The determination of the present-day lithospheric structure represents the basis for any evolutionary model of the Earth (Rudnick & Fountain 1995; Rudnick *et al.* 1998; Artemieva & Mooney 2001; Lee 2003; Eaton *et al.* 2009; Fischer *et al.* 2010; Hopper *et al.* 2014). One of the main goals concerning the Earth's outermost structure is to provide crucial information not only for interpreting lithospheric features (Rychert & Shearer 2009), but also how the lithospheric–sublithospheric system would respond to perturbations arising from tectonic shortening (Molnar *et al.* 1998; Jadamec *et al.* 2013; Sharples *et al.* 2015), rifting (Daradich *et al.* 2003; Liu *et al.* 2004; Sharples *et al.* 2015), and sublithospheric convection (King & Ritsema 2000). In this context, a detailed knowledge of the structure of the lithosphere is an essential requirement for understanding (1) the relationship between surface characteristics and deep processes, (2) the physical interactions between the lithosphere and sublithospheric mantle flow (Conrad *et al.* 2007; Flament *et al.*

2013; Jadamec 2016a; MacDougall *et al.* 2017), (3) the origin and evolution of the lithosphere (Herzberg & Rudnick 2012) and (4) the nature of the lithosphere–asthenosphere coupling (Jadamec & Billen 2010; Jadamec 2016b).

Global lithospheric studies have provided reliable upper mantle structure around the world showing variations in depth to the lithosphere–asthenosphere boundary (LAB) and in the physical properties within the lithosphere, such as lithospheric strength, density and temperature distribution (Artemieva & Mooney 2001; Artemieva 2006; Eaton *et al.* 2009; Rychert & Shearer 2009; Fischer *et al.* 2010, Lekic & Romanowicz 2011; Tesauro *et al.* 2012). These studies show LAB thickness variations from oceans to continents at broad wavelengths (about 1000 km). However, both the absolute depth and the nature of the boundary are debated. Where additional data are available, regional LAB models can provide finer resolution and can help to constrain the detailed regional structure (Fullea *et al.* 2010, 2014; Jadamec *et al.* 2013; Jones *et al.* 2014; Carballo *et al.* 2015a, b; Torne *et al.* 2015; Tunini *et al.* 2016).

In mainland Alaska and the western offshore domains, the depth to the LAB has been determined in part by global and continental scale models of the thermal lithosphere (e.g. Artemieva 2006) and by seismic tomography studies (e.g. Simmons *et al.* 2012; Schaeffer & Lebedev 2013a, b) that provide broad scale information. Local efforts as a part of the Trans-Alaska Crustal Transect (TACT) have provided constraints on the crustal and lithospheric structure along the center line of mainland Alaska, from Prince William Sound to the south to Prudhoe Bay to the north (e.g. Fuis *et al.* 2008). More recently, a local model based on *S*-wave receiver functions (SRF) has added detailed information on the base of the seismic lithosphere mainly in the eastern region of mainland Alaska (O'Driscoll & Miller 2015), but does not constrain the structure where the lithosphere continues NW and W into the Chukchi Shelf, Inner and Outer Bering shelf and into the easternmost Chukchi Peninsula in Russia (Fig. 1). First-order efforts to characterize the regional thermal and/or lithospheric structure in Alaska have also been undertaken as a part of geodynamic modelling studies (e.g. Bird 1996; Kalbas *et al.* 2008; Jadamec & Billen 2010; Jadamec *et al.* 2013) based on the varying levels of synthesis of geological and geophysical observations, such as surface heat flow (Batir *et al.* 2016), seismic profiles (Fuis *et al.* 2008), terrane boundaries (Greninger *et al.* 1999) and/or constraints from the thermal models of the Canadian cordillera (Lewis *et al.* 2003).

Previous studies have also aimed to resolve the crustal structure for different regions of the Alaska mainland and offshore domains. Active source experiments, seismic tomography imaging, and analysis of receiver functions together with the recent deployment of the US Transportable Array (TA) have allowed mapping out the Moho topography of onshore Alaska in more detail. The Trans–Alaska Crustal Transect (TACT) active source experiment was an early study that provided a seismic transect across Alaska from the southern subduction zone boundary to the North Slope (Fuis *et al.* 2008, and references therein). Additional information comes from broad-band seismic imaging of the BEARR, MOOS and STEEP broad-band networks (e.g. Ferris *et al.* 2003; Eberhart–Phillips *et al.* 2006; Rossi *et al.* 2006, and references therein). Wang & Tape (2014) present a Moho map of central and southern Alaska, south of 68°N from the compilation of seismic and gravity data on land and from the global crustal model Crust 2.0 (Bassin 2000) in the offshore areas. More recently, a Moho map from *P*-wave receiver functions (PRF) has been extended to the west using all available broad-band stations including the USArray (Miller & Moresi 2018; Miller *et al.* 2018). Offshore, information of the crustal architecture of the Bering and Chukchi shelves mainly comes from the compilation of the 3750 km crust–penetrating marine seismic reflection profiles from Klemperer *et al.* (2002). Local crustal information in the region of the subducting Yakutat plateau comes from the onshore–offshore active seismic STEEP experiment (Worthington *et al.* 2012; Christeson *et al.* 2013).

Compilation of the aforementioned data sets shows that in spite of the tremendous efforts, there are still uncovered areas, particularly in the northern onshore and offshore regions, where the location of permanent broad-band stations is very limited. Thus, the main objective of this work is to extend the existing partial crustal thickness models of mainland Alaska into western Alaska, the eastern Aleutian Islands, the Chukchi Shelf, Inner and Outer Bering shelf and the easternmost Chukchi Peninsula and to investigate the topography of the thermal LAB over this region.

To that purpose, we present a regional model of the lithospheric structure based on joint modelling of elevation and geoid height data together with thermal analysis. We also perform 3-D forward and inverse modelling of Bouguer gravity anomalies to validate the obtained lithospheric structure, to analyse areas that depart from local isostasy, and to map crustal density heterogeneities. The method follows from that applied to estimate the crustal and lithospheric mantle geometry in a variety of tectonic settings, for example the Gibraltar Arc System (Fullea *et al.* 2007), the Arabia–Eurasia collision zone (Jiménez–Munt *et al.* 2012), Central Asia (Robert *et al.* 2015), the Iberian mainland (Torne *et al.* 2015) and the African continent (Globig *et al.* 2016).

2 GEOLOGICAL HISTORY AND TECTONOSTRATIGRAPHIC TERRANES

Tectonically, the Alaska mainland bridges the Cordillera orogenic belt of western North America and the belts of the Arctic realm (Nokleberg *et al.* 1994; Moore & Box 2016). The region is bounded to the north by the Canadian Basin and to the south by the Aleutian–Alaska subduction zone (Fig. 1). A full description of the lithology, detailed terrane nomenclature subdivisions, and geological and tectonic history of the more than 100 terranes in Alaska is beyond the scope of this study. The summary below is based primarily on the detailed work in Kirschner (1992), Nokleberg *et al.* (1994), Klemperer *et al.* (2002), Moore & Box (2016) and more recent summaries in Miller *et al.* (2017). For further details, the reader is also referred to Jones *et al.* (1981), Plafker & Berg (1994), Greninger *et al.* (1999), Nokleberg (2000) and Fuis *et al.* (2008).

The lithospheric structure of Alaska has been shaped by a long and complex tectonic history comprised of the amalgamation of terranes of varying origin, deformational episodes and timing of accretion, with the modern landmass fully assembled by the Late Cretaceous (Jones *et al.* 1981; Nokleberg *et al.* 1994; Plafker & Berg 1994; Fuis *et al.* 2008, Moore & Box 2016). The amassed terranes include continental remnants of Laurentia, Baltica and Siberia as well as various tectono-stratigraphic lithologies indicative of oceanic plate, magmatic arc, island arc and broader subduction zone affinities (Jones *et al.* 1981; Nokleberg *et al.* 1994; Plafker & Berg 1994; Fuis *et al.* 2008, Moore & Box 2016).

Based on the extensive synthesis of numerous field studies and geological data, the study region can be divided into three broad domains that each have different deformational histories and tectonic origin (Nokleberg *et al.* 1994; Fuis *et al.* 2008; Moore & Box 2016). The northern domain encompasses the Chukchi and Beaufort shelves, the North Slope of Alaska and the Brooks Range and

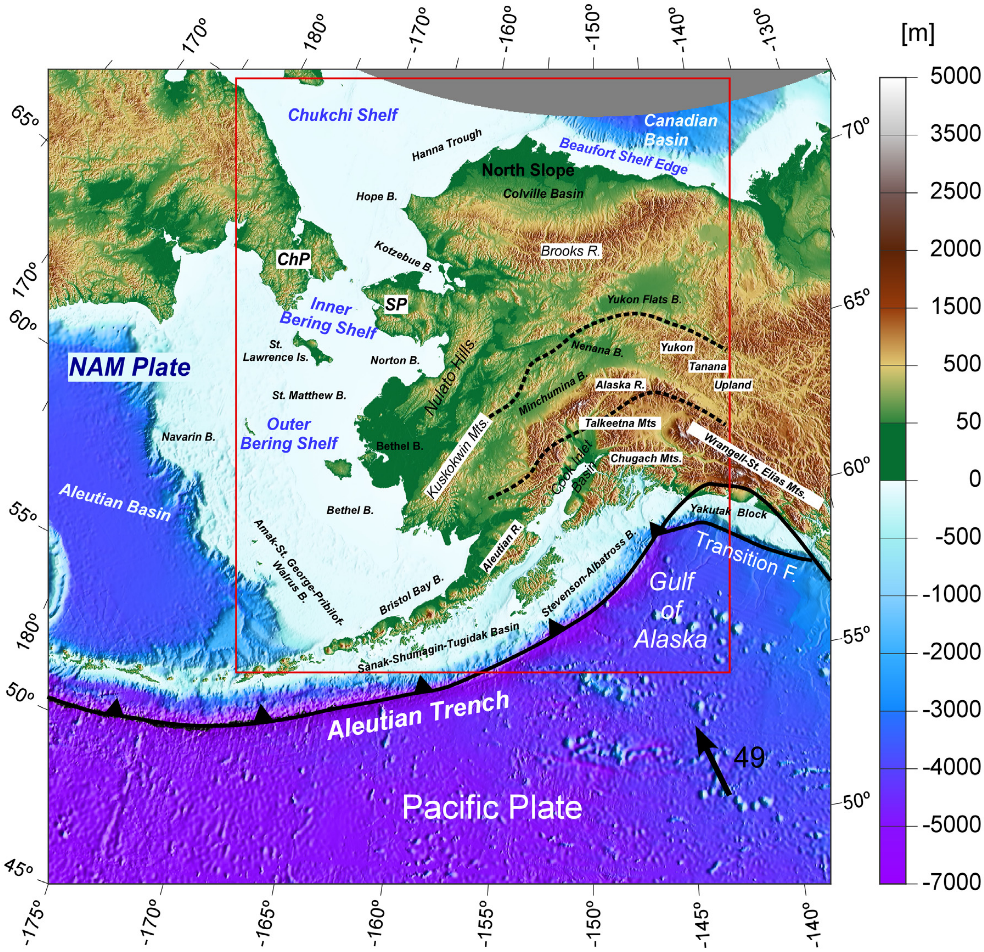

Figure 1. Location map, with study area highlighted by red square. Black thick line shows the Aleutian subduction zone. Dark grey shows the Transition Fault. ChP: Chukotka Peninsula. NAM: North American Plate. SP: Seaward Peninsula. B.: basin; Mts.: mountains; F.: Fault; R.: range. Black arrow: Pacific Plate motion in mm yr^{-1} relative to North America. Black dashed lines outline deformational domains of Alaska as defined by Moore & Box (2016).

NE Russia. The interior domain comprises the onshore region between the Tintina and Denali faults and the offshore Inner Bering shelf. The southern domain encompasses the region south of the Denali Fault and the offshore Outer Bering shelf (Nokleberg *et al.* 1994; Klemperer *et al.* 2002; Fuis *et al.* 2008; Moore & Box 2016, Figs 1 and 2).

The northern domain includes the Arctic–Alaska terranes and the oceanic affinity Koyukuk terranes accreted to Alaska during the Early Cretaceous oceanic arc–continent collision (Brookian orogeny) and mid–Cretaceous extension. The Late Jurassic and Early Cretaceous arc–continent collision resulted in the emplacement of the Angayucham–Tositna–Innoko terrane (ATI) and Koyukuk oceanic terranes onto the continental domain, in subduction related metamorphism in the underthrusted terranes, and folding and thrusting of the sedimentary cover units.

The Interior domain comprises the Yukon Composite and Farewell terranes and a number of smaller terranes (Nokleberg *et al.* 1994; Fuis *et al.* 2008; Moore & Box 2016). The Yukon Composite terrane mainly consists of ductilely deformed Proterozoic–to–Palaeozoic metamorphic rocks having strong affinities with rocks of the North American craton and overlying arc–related rocks in the east–central and southern regions that were tectonically transported to the Alaska landmass. According to Plafker & Berg (1994), and references therein, these rocks record a first episode of Late Devonian and mid–Cretaceous arc–related continental margin magmatism followed by arc magmatism in the late Palaeozoic and in the Late Triassic and Middle Jurassic. From the Late Triassic to Middle Cretaceous the domain experienced major episodes of regional plutonism and metamorphism in mainland and southeast Alaska; accretion of the Yukon Composite terrane against the continental margin during the early Middle Jurassic and mid–Cretaceous plutonism and crustal extension in east–central Alaska and adjacent areas.

The Southern domain consists of two generalized styles of tectonic units, the primarily arc related Peninsular, Wrangellia and Alexander terranes (herein referred as the Wrangellia Composite terrane) and the primarily accretionary complex related terranes (Chugach and Prince William terranes) located outboard, including the actively accreting/subducted oceanic Yakutat plateau terrain (e.g. Worthington *et al.* 2012, and references therein).

Onshore, the accreted terranes are separated by deep sedimentary basins, some of them floored by narrow strips of oceanic crust that were likely consumed by subduction starting in the Middle-Late Jurassic. Although the detailed geology is still challenging, it is important to note that a number of north-dipping thrust faults are interpreted along the northern sides of both the Alaska and Brooks

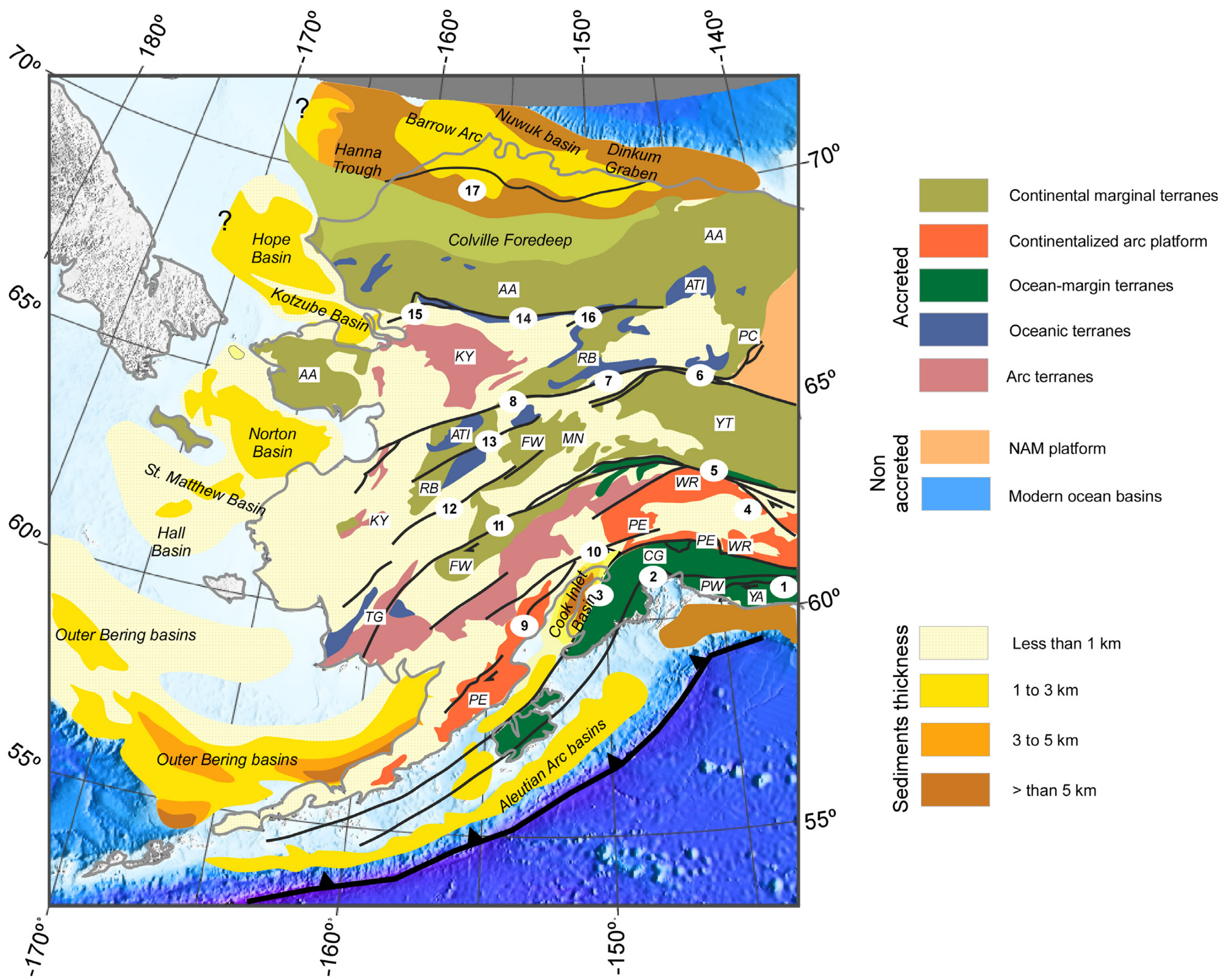

Figure 2. Terrane map of Alaska simplified from Nokleberg *et al.* (1994), Plafker *et al.* (1994), Moore & Box (2016) and Kirschner (1992). Major Cenozoic strike–slip faults–1: Chugach–St. Elias; 2: Contact; 3: Border Ranges; 4: Totschunda; 5: Denali; 6: Tintina; 7: Victoria Creek; 8: Kaltag; 9: Bruin Bay; 10: Castle Mountain; 11: Farewell; 12: Iditarod; 13: Poorman; 14: Southern Brooks Range extensional fault system; 15: Kobuk; 16: South Fork; 17: Brooks Range deformation front. Terranes—AA: Arctic–Alaska; ATI: Angayucham–Tozitna–Innoko; CG: Chugach; FW: Farewell; KY: Koyukuk; MN: Minchumina; PC: Porcupine; PE: Peninsular; PW: Prince William; RB: Ruby; TG: Togiak; WR: Wrangellia; YA: Yakutat; YT: Yukon–Tanana.

ranges (Coney & Jones 1985; Fuis *et al.* 2008). This northern structural vergence could indicate the potential southern subductions of small oceanic basins between distinctive terranes.

The long-lasting subduction of the Pacific Ocean lithospheric slab produced profuse magmatism in Wrangellia with a sequence of pluton intrusions migrating northwards from Middle Jurassic to early Late Cretaceous periods (Moore & Box 2016). According to these authors, there was a backward shift of magmatic intrusions towards the central part of Alaska contributing to the growth of the Wrangell arc during latest Cretaceous times (Campanian–Maastrichtian). This plutonic shift coincided with the deformation of the central sector of Alaska and preceded a second phase of significant widespread tectonic compression along central Alaska and the Brook Range and adjacent foreland basin (Moore & Box 2016).

Furthermore, the continued subduction of the Pacific Ocean under Alaska led to the growth of voluminous accretionary prisms along the front of the Alaskan upper plate. These are separated in three tectono-sedimentary complexes that from oldest to youngest are the McHugh Complex, the Valdez Group, and the Orca Group (Trop & Ridgway 2007). The last significant episode was the subduction at the end of the Oligocene of the Yakutat block, a large oceanic plateau, along the hinge zone between the Aleutian trench and the Fairweather-Queen Charlotte transform fault (Bruns 1983; Ferris *et al.* 2003; Eberhart–Phillips *et al.* 2006; Enkelmann *et al.* 2009; Worthington *et al.* 2012). The buoyant nature of the Yakutat block may have triggered the flattening of the subducting slab (Ratchkovski & Hansen 2002; Ferris *et al.* 2003; Pavlis *et al.* 2004), and is currently indicated by the large earthquakes hitting this hinge region but also affecting the entire interior Alaska.

Tectonic compression and plutonic intrusions have given rise to impressive mountain ranges, with the highest Denali peak (granitic pluton) reaching 6190 m in the Alaska Range (Fitzgerald *et al.* 1995; Jadamec *et al.* 2013). The ranges south of the Kaltag and Tintina faults are arcuate and clearly parallel the curved geometry of the hinge zone, corresponding to the Gulf of Alaska. It is interesting to note that the combined geometry of these ranges together with the set of dextral faults that characterize Alaska (Yukon-Tanana–Tintina Fault, Alaska Range-Wrangel St Elias Mountain–Denali Fault and

Chugach Mountains–Chugach–St Elias Fault) have a common tectonic pattern mimicking the current Aleutian Trench-Queen Charlotte transform fault (Figs 1 and 2). This repeated tectonic hinge region could nucleate the formation of the compressive mountain ranges, the topography and therefore the associated tectonics that decrease westwards plunging under large sedimentary basins and under the Bering and Chukchi continental shelves (Figs 1 and 2).

3 METHODS

The regional crustal and lithospheric structure models for Alaska and adjacent shelves are calculated by combining elevation, geoid height data and thermal analysis. The models assume thermal steady-state and local isostasy. In addition, to analyse departures from local isostasy and density heterogeneities at crustal levels, we compute the 3-D gravity effect of the resulting lithospheric structure and subtract it from the observed Bouguer anomaly to separate its regional and local components. We then invert the obtained 3-D residual anomalies to highlight crustal lateral density variations over the model domain.

3.1 Crust and lithosphere modelling

3.1.1 Calculation of crustal thickness and depth to the LAB

We calculate a regional model of the crust and lithospheric mantle thickness for Alaska and the adjacent continental shelves that is compatible with elevation and geoid observations. The model domain extends from approximately –185° to –135° west longitude and from 55° to 72° north latitude, with a spatial resolution of 5 × 5 km. It spans mainland Alaska and the eastern Aleutian Islands, and extends westward onto the Chukchi Shelf, Inner and Outer Bering shelf, as well as onto the easternmost Chukchi Peninsula in Russia (Fig. 1).

The thickness of the crust and mantle lithosphere are calculated on the model grid by joint modelling of elevation and geoid height data, together with thermal analysis, using the methodology developed by Fullea *et al.* (2007). Assuming local isostasy, the elevation, ε is proportional to $\int\rho(z)\cdot dz$ and the geoid height, N, is proportional to $\int z\cdot\rho(z)\cdot dz$, where $\rho(z)$ is the density at depth (z). Both integrals extend from the Earth's surface to the compensation level; from the actual topography for $\varepsilon \geq 0$ and to sea level for $\varepsilon < 0$, and to the deepest point of the LAB over the modelled region.

The elevation, ε, relative to sea level can be calculated from (Lachenbruch & Morgan 1990):

$$\varepsilon = (\rho_a - \rho_L)/\rho_a \cdot L - L_0 \qquad (\varepsilon \geq 0) \qquad (1a)$$

$$\varepsilon = \rho_a/(\rho_a - \rho_w) \cdot ((\rho_a - \rho_L)/\rho_a \cdot L - L_0) \qquad (\varepsilon < 0) \qquad (1b)$$

where ρ_a is the density of the asthenosphere, ρ_L is the average density of the lithosphere, ρ_w is the density of seawater, L is the total lithospheric thickness and L_0 is the depth of the free (unloaded) asthenospheric level (2320 m, Fullea *et al.* 2007). The densities of seawater and the asthenosphere given in Table 1, and the reference lithosphere is described below.

The geoid anomaly, N, can be calculated as (Haxby & Turcotte 1978):

$$N = -2\pi G/g \int z \cdot \rho(z) \cdot dz + N_0, \qquad (2)$$

where G is the universal gravity constant, g is the gravitational acceleration due to gravity at the Earth's surface, $\rho(z)$ is the density at depth (z) and the integration constant, N_0, is a reference value to which the calculated N-values are referred.

Eqs (1) and (2) are solved simultaneously assuming a four–layer model composed of water, crust, lithospheric mantle and asthenosphere, with known densities (Table 1). The densities of water and the asthenosphere are kept constant (Table 1). We assume the crustal density is laterally homogeneous and increases linearly with depth from 2670 kg m^{-3} at the surface to 2950 kg m^{-3} at the base of the crust, which results in an average crustal density of 2810 kg m^{-3} (Table 1). The density of the lithospheric mantle is considered to be temperature dependent such that

$$\rho_m(z) = \rho_a \ (1 + \alpha [T_a - T_m(z)]) \qquad (3)$$

where $\rho_m(z)$ and $T_m(z)$ are the density and temperature of the lithospheric mantle at depth z, respectively, and ρ_a and T_a are the density and temperature of the asthenosphere, respectively (e.g. Lachenbruch & Morgan 1990, Table 1). The temperature, T, distribution is calculated by solving the 1-D heat transport equation for steady state

$$k \cdot \nabla^2 T + A = 0, \qquad (4)$$

where k is the scalar thermal conductivity, ∇^2 is the Laplace operator, A the volumetric heat production and fixed temperature boundary conditions are used at the model surface and the LAB, with values given in Table 1.

Table1. Model input parameters.

The seismic data used to constrain the reference lithospheric column to which the calculated geoid height values are referred are described in Section 3.2. A key aspect in deriving the crust and lithospheric mantle geometries from geoid and elevation data is the value of the integration constant N_0 in eq. (2), which is obtained from a reference lithospheric column, where the geoid height N and the crustal and lithospheric mantle thicknesses and their respective densities are known. Following Globig *et al.* (2016), we have chosen the reference column that best fits the crustal thickness data obtained from seismic experiments for the whole study region. This column consists of a 35-km-thick crust and a 172-km-thick lithosphere with densities described in Table 1 that result in an elevation of 0 m above sea level and $N_0 = 6170$ m.

Note that the thermal parameters mainly influence the calculated Moho temperatures, which in turn modify the density of the lithospheric mantle. According to the sensitivity analysis made by Fullea *et al.* (2007), the LAB depth decreases almost linearly with increasing the thermal expansion coefficient (α) and crustal thermal conductivity (k_c), and by decreasing the radiogenic heat production (H_s). These authors conclude that the LAB depth is mostly affected by α ($\leq$12 km) and to a lesser extent, by H_s and k_c ($\leq$8 km), and that decreases almost linearly with increasing α and k_c, and decreasing H_s values. In addition, they also found that the Moho depth is not much affected ($\sim$1 km) by variations of any of the thermal parameters. Similarly, the obtained lithospheric structure depends also on the selected values for the average crustal density and N_0. Different pairs of $\overline{\rho_c}$ and N values can also fit the measured crustal thickness data but resulting in less reliable lithospheric thickness when compared to tomography studies.

Table 1. Parameters used in crust and lithosphere models. Average crustal density is 2810 (kg m^{-3}). Models assume a surface temperature, T_s, of 0 °C and temperature at the lithosphere–asthenosphere boundary, T_a, of 1330 °C. The coefficient of thermal expansion, α, is a constant value of 3.5×10^{-5} K^{-1}.

	Heat production (A) (μW m^{-3})	Thermal conductivity (k) (W (K · m)$^{-1}$)	Density (ρ) (kg m^{-3})
Continental crust	0.8	2.5	Increases linearly with depth
Oceanic crust	0.3	2.1	Increases linearly with depth
Lithospheric mantle	0.0	3.2	Calculated in eq. (3)
Sea water	-	-	1030
Top of crust	Same as above	Same as above	2670
Base of crust	Same as above	Same as above	2950
Asthenosphere	-	-	3200

3.1.2 Calculation of 3-D Bouguer anomaly and crustal density variations

A predicted regional 3-D Bouguer anomaly is then calculated for the entire region based on the crust and mantle lithosphere geometry obtained in Section 3.1.1. This regional Bouguer anomaly is calculated in 3-D using GeoMod3D (Jiménez-Munt *et al.* 2011), which is a modified version of the finite differences code LitMod3D (Fullea *et al.* 2009). GeoMod3D considers a number of right rectangular flat-topped prisms centered in each node of the finite difference grid. Each lithospheric column is decomposed into different vertical prisms according to the number of existing layers. For each prism, a linear density gradient is considered. The gravity anomalies in every surface point of the model are calculated using the analytical expression in 3-D cartesian coordinates of Gallardo-Delgado *et al.* (2003). Densities of the four relevant layers (water, crust, lithosphere mantle and asthenosphere) are taken as in step one (Table 1).

The average crustal density variations in the study region are then calculated to reproduce the residual gravity anomalies obtained from subtraction of the regional gravity field calculated above from the observed Bouguer anomaly. For this purpose, we used the GMSYS-3D commercial software (Popowski *et al.* 2005) that allows us to invert a gravity signal by fixing the top and bottom of the causative layer and varying its average density. Here, we assume that the anomalous bodies causing the residual gravity anomalies are distributed within the crust (Torné *et al.* 2015).

3.2 Geophysical characteristics and constraints used in study

A detailed description of the geophysical data sets used in this study is provided in the following sections.

3.2.1 Elevation constraints

Elevation data from topo_19.1.img (*https://topex.ucsd.edu/pub/global_topo_1 min/*) (Sandwell & Smith, 1997, updated) show a varied topographic landmass (Fig. 3a). Onshore, maximum average elevation values are attained in southern Alaska, along the Alaska Range, Talkeetna Mountains and Chugach-St. Elias mountains, with local values up to 6000 m (Fig. 1). In the north, the Brooks Range shows values above 1500 m, gently decreasing to the west as they approach the shoreline. Intermediate values (from 500–1000 m) are observed along the Nulato Hills and Kuskokwin Mountains, whereas the lowlands show elevations below 500 m. Offshore, the Bering and Chukchi seas are characterized by shallow waters (above –500 m), except in the Aleutian and Canadian basins where the ocean floor deepens to as much as –2000 and –3000 m, respectively. Depths of more than 3000 m are reached in the SE–most corner in the Gulf of Alaska, with narrower deeper regions along the Alaska-Aleutian trench, and broader regions of depths greater than 5000 km southwest of the study area (Fig. 3a).

Assuming that elevation short-wavelengths are supported by the rigidity of the lithosphere, in our study, the elevation signal is filtered by applying a low-pass Gaussian filter of 80 km to avoid unrealistic short-wavelength effects.

3.2.2 Bouguer anomaly

The Bouguer anomaly map shown in Fig. 3(b), covering onshore and offshore regions, is derived from the Free Air anomaly satellite data compilation by Sandwell *et al.* (2014) (*https://topex.ucsd.edu/pub/global_grav_1 min/*) applying the complete Bouguer reduction using the FA2BOUG code of Fullea *et al.* (2008) with a reduction density of 2670 kg m^{-3}. Onshore, the Bouguer anomaly map shows prominent regional lows, in the range of –140 to –60 mGal, that frame the mountainous regions of southern Alaska and the Brooks Range to the north, indicating crustal thickening. The northern low extends north of the Brooks Range into the northeastern Brooks Range and the late Mesozoic and Cenozoic foredeep Colville Basin, where values in the range of –60 to –20 mGal are observed. In contrast, the Beaufort Sea to the north is framed by a gravity high that locally reaches values of 180 mGal. The onshore lowlands and the offshore continental platforms of the Bering and Chukchi seas show values in the range of –20 to 20 mGal, suggesting a thinner crust underneath. At the southern boundary of the North American Plate in Alaska, a sharp gradient, parallel to the coast marks the transition from the Aleutian subduction zone to the oceanic crust of the Pacific Plate. A prominent local gravity low (up to –140 mGal) characterizes the northeast-trending collisional forearc Cook Inlet Basin (Fig. 1), with large hydrocarbon accumulations and significant thicknesses of Mesozoic to Cenozoic sediments.

3.2.3 Geoid model

Geoid height data come from the GECO global model (Gilardoni *et al.* 2016, Fig. 3c). The GECO gravitational model includes spherical harmonic coefficients up to degree and order 2190. In order to remove the deep sublithospheric mantle signal, we have filtered the

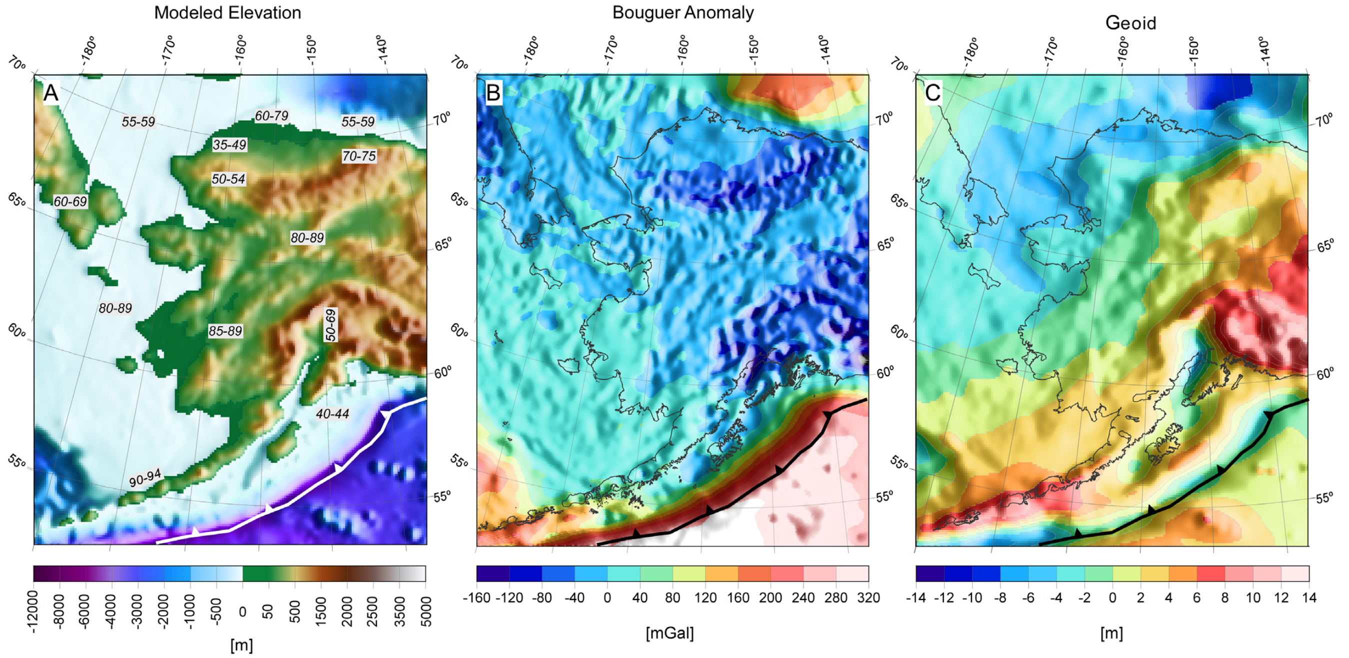

Figure 3. (a) Elevation data from topo_19.1.img (https://topex.ucsd.edu/pub/global_topo_1 min/) (Sandwell & Smith, 1997, updated) after removing wavelengths <80 km using a Gaussian filter. Numbers are heat flow values in mW m^{-2}. (b) Bouguer anomaly map of the onshore and offshore regions derived from the Free Air anomaly satellite data compilation by Sandwell *et al.* (2014) (https://topex.ucsd.edu/pub/global_grav_1 min/). Density reduction is 2670 kg m^{-3}. (c) Geoid anomaly map from GECO Global Model (Gilardoni *et al.* 2016). Long wavelengths have been removed by subtracting spherical harmonics up to degree and order 12 from the total geoid. A low-pass Gaussian filter of 80 km has been applied to remove short-wavelengths effects. Shading indicates elevation. See text for details on Bouguer and geoid anomaly reduction.

signature corresponding to the lower spherical harmonics until degree and order 12. Thus, we retain the effects of density anomalies shallower than 400 km depth, avoiding the effects of undesired sub-lithospheric density variations (Root *et al.* 2015). For consistency with the modelled elevation data we have filtered the short wavelength components of the geoid by applying a low-pass Gaussian filter of 80 km.

The obtained geoid anomalies show a regional trend across Alaska of values decreasing from the SE to NW with maximum values, in the range of 2–12 m, along the westernmost end of the Alaska Peninsula and east of the Cook Inlet basin. Noteworthy is the presence of a conspicuous NW–SE elongated geoid high east of 150°W that encompasses the eastern Wrangellia, Prince William and Chugach Terranes (Fig. 3c). To the north, the eastern segment of the Brooks Range is characterized by a relative high (locally up to 6 m); however, its western segment shows a gentle decrease of geoid values from 2 to –4 m. This decrease is partly associated with the lowering of elevation and partly to the presence of a regional geoid low (from –2 to locally –10 m) that could mask the surficial geoid signature. The regional low that covers NW Alaska and the Chukchi and Beaufort seas is likely related to density anomalies at lithospheric mantle levels.

3.2.4 Seismic data constraints

Crustal seismic information used in this study (Fig. 4) comes from reflection and refraction surveys collected between 1983 and 1990 along the TACT line that extends from the Aleutian Trench to the Arctic coast (Fuis *et al.* 2008, and references therein) and from the analyses of PRF of Miller *et al.* (2018) and Miller & Moresi (2018). Additional local data have been taken from the compilation of Wang & Tape (2014) that includes data from Ai *et al.* (2005) and Rossi *et al.* (2006). Seismic data offshore of western Alaska come from the compilation of Klemperer *et al.* (2002) along a 3750-km-long deep marine seismic–reflection transect. Regional LAB information has mainly been taken from the *S*-wave receiver function model of O'Driscoll & Miller (2015).

In terms of overall patterns of crustal thickness from previous studies, the Brooks Range and its northwestern termination are characterized by relatively thick crust (>45 km, e.g. Fuis *et al.* 2008; Miller & Moresi 2018; Miller *et al.* 2018). Partof the observed crustal thickening may be due to lower crustal duplexing, with either northern or southern vergence that is still under debate (Fuis *et al.* 1997). South of the Brooks Range, these studies suggest interior Alaska is characterized by an average crustal thickness of approximately 35 km (Fig. 4). Thinner values have been predicted in the Seward Peninsula, southeast of the eastern Brooks Range, and north of the central Alaska Range (Fig. 4). A notable observation is the relative abrupt change in crustal thickness across the Denali fault, where large variations of Moho values occur over short distances likely due to the history of terrane accretion and variation in terrane composition and deformation history (e.g. Eberhart-Phillips *et al.* 2006; Veenstra *et al.* 2006; Fuis *et al.* 2008; O'Driscoll & Miller 2015). Seismic data also show that the thicker crustal values on the south side of the Denali fault continue southward toward the trench (e.g. Miller *et al.* 2018). However, in the Prince William sound and Kenai Peninsula regions, thick crust in the upper plate is unlikely as the subduction zone is characterized by the modern flat slab occurring at shallow depths, requiring thin crust in the upper plate south of Anchorage (Ratchkovski & Hansen 2002; Jadamec & Billen 2010; Wang & Tape 2014; Hayes *et al.* 2018; Jadamec *et al.* 2018).

Offshore western Alaska, Klemperer *et al.* (2002), based on deep seismic reflection profiling, report a relatively deep multichannel

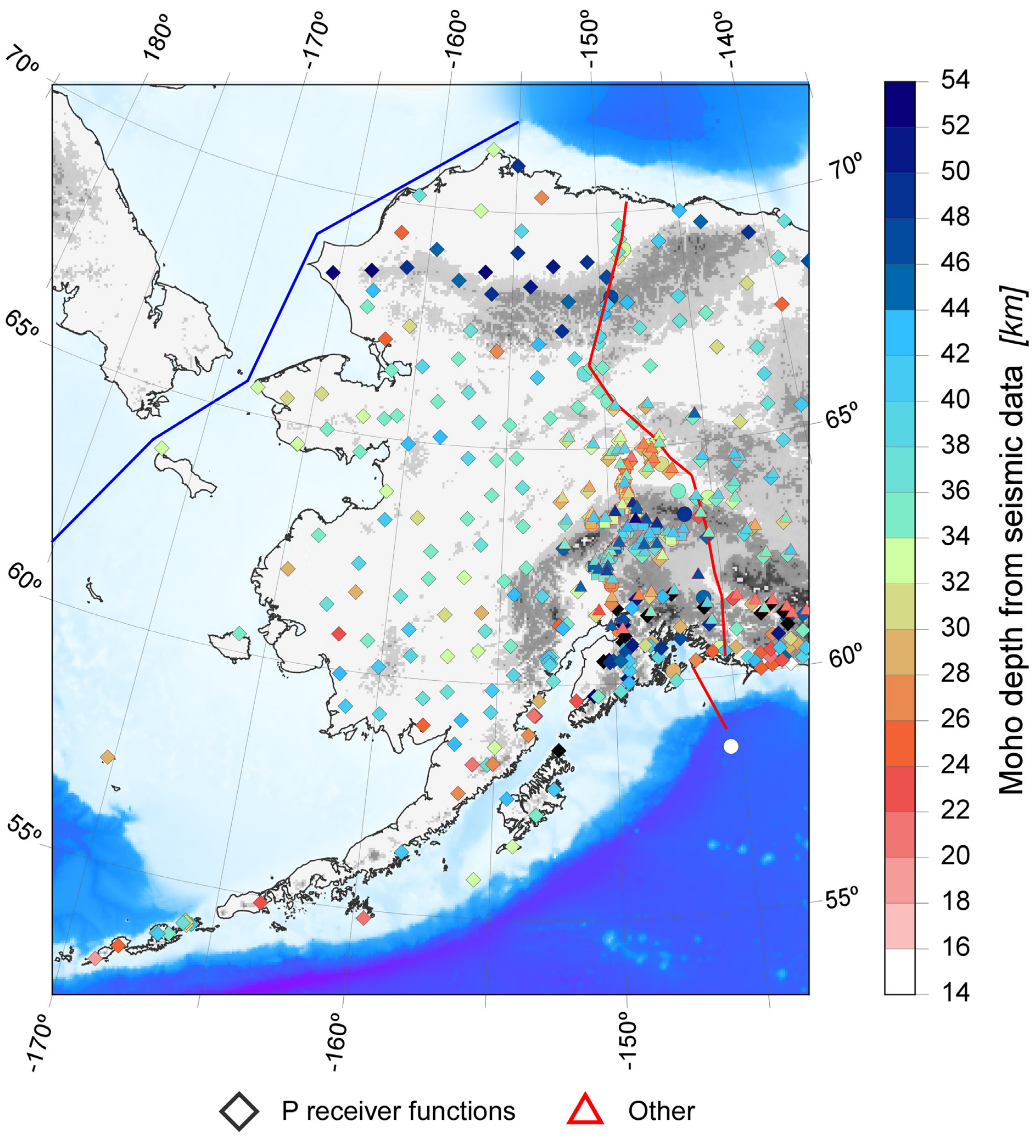

Figure 4. Seismic data collected to constrain the crustal model. Diamonds indicate RF analyses from Miller *et al.* (2018) and Ai *et al.* (2005), Miller & Moresi (2018) and Rossi *et al.* (2006). Triangles indicate seismic data from other authors (see Section 3.2.4 for a complete reference list). The onshore red thin line shows the location of the Trans Alaska Transect (Fuis *et al.* 2008). The offshore blue line shows the location of the regional marine seismic–reflection profiles gathered by Klemperer *et al.* (2002). Grey and coloured background show topography and bathymetry, respectively.

seismic reflection Moho (>12 s TWTT–two-way traveltime) underneath the Arctic–Alaska Crustal Province (see their fig. 2) shallowing from the southern half of the Kotzebue basin to north of St. Matthew Island where values are between 10 and 11 s TWTT. Further discussion of seismic data and comparison with our modelling results is given in Section 5.

4 RESULTS

In this section, we present the lithosphere structure, and residual gravity and densities obtained in this study for the Alaska mainland, the eastern Aleutian Islands, the Chukchi Shelf, Inner and Outer Bering shelf and the easternmost Chukchi Peninsula in Russia (Figs 5–7). The model domain extends over 10° in latitude and over 20° in longitude and comprises the northwestern most portion of the North American Plate.

4.1 Crustal structure in mainland Alaska and adjacent continental shelves

Fig. 5 shows the crustal thickness for the study region obtained from our modelling approach using the parameters summarized in Table 1. In the onshore Northern region, the highest relief of the Brooks Range is characterized by a crustal root with values above 39 km and up to 45 km in the NE-most corner, whereas in its western segment there is a progressive thinning towards the shoreline, coinciding with a decrease of the topographic relief (Fig. 3a).

From south of the Brooks Range to north of the Denali and Farewell faults we obtained a moderately thick crust from 34 to 36 km. Minimum values are obtained in the lowlands and basins (e.g. Yukon Flats Basin), while the maxima delineate the relative mid-ange elevation of the Kuskokwim Mountains, the Nulato Hills in the east and the Yukon–Tanana Upland in the west (Figs 1 and 5).

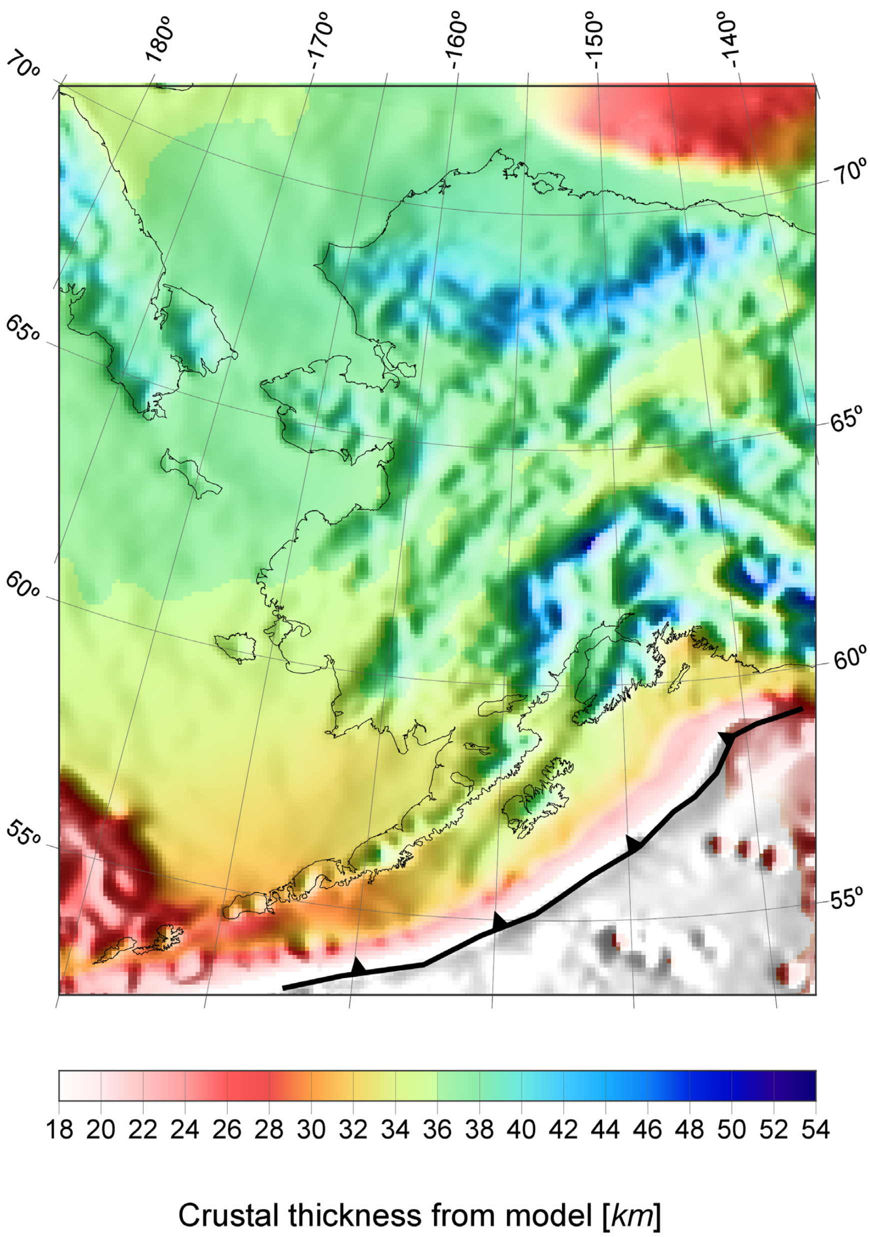

Figure 5. Crustal thickness map obtained from joint modelling elevation and geoid data, together with thermal analysis. Colour key shows depth to the base of the crust. Contours every 2 km. Shading indicates elevation.

Further to the south, the Denali fault clearly marks an abrupt change in the crustal structure observed both for surficial and deep levels. The most striking feature is the conspicuous arc-shaped crustal thickening of the southern mountain belts. Overall, the crustal thickness in the Alaska Range and Wrangell and Chugach Mountains varies on average between 38 and 44 km, showing local spots with thickness up to 52 km that coincide with elevation highs. South of the Chugach Mountains, there is a progressive eastward crustal thinning that reaches values up to 22–24 km on the slope break. Along the continental shelf, we obtain average values of ∼ 30 km.

Offshore western Alaska, we observe an anomalously thick crust (>36 km) relative to the shallow bathymetry of the area, that extends from southern St Lawrence Island latitude to the Chukchi Shelf (Figs 1 and 5).

4.2 LAB structure in mainland Alaska and adjacent continental shelves

Fig. 6 shows the lithospheric thickness map for the study region obtained from our modelling approach. Our LAB results show that north of the Denali Fault there is a regional northwest directed lithospheric thickening ranging from minimum values of 150 km to more than 180 km. The lithospheric root from 180 to 200 km extends throughout the northern region covering the Chukchi and Beaufort shelves, the North Slope of Alaska, most of the Brooks Range and Chukotka Peninsula, coinciding with the proposed position of the Chukotka-Artic Alaska microplate as defined by Shephard *et al.* (2013) (Fig. 6). Offshore the regional trend is even more visible as it extends from the Aleutian Arc to the Chukchi Sea and NE Russia.

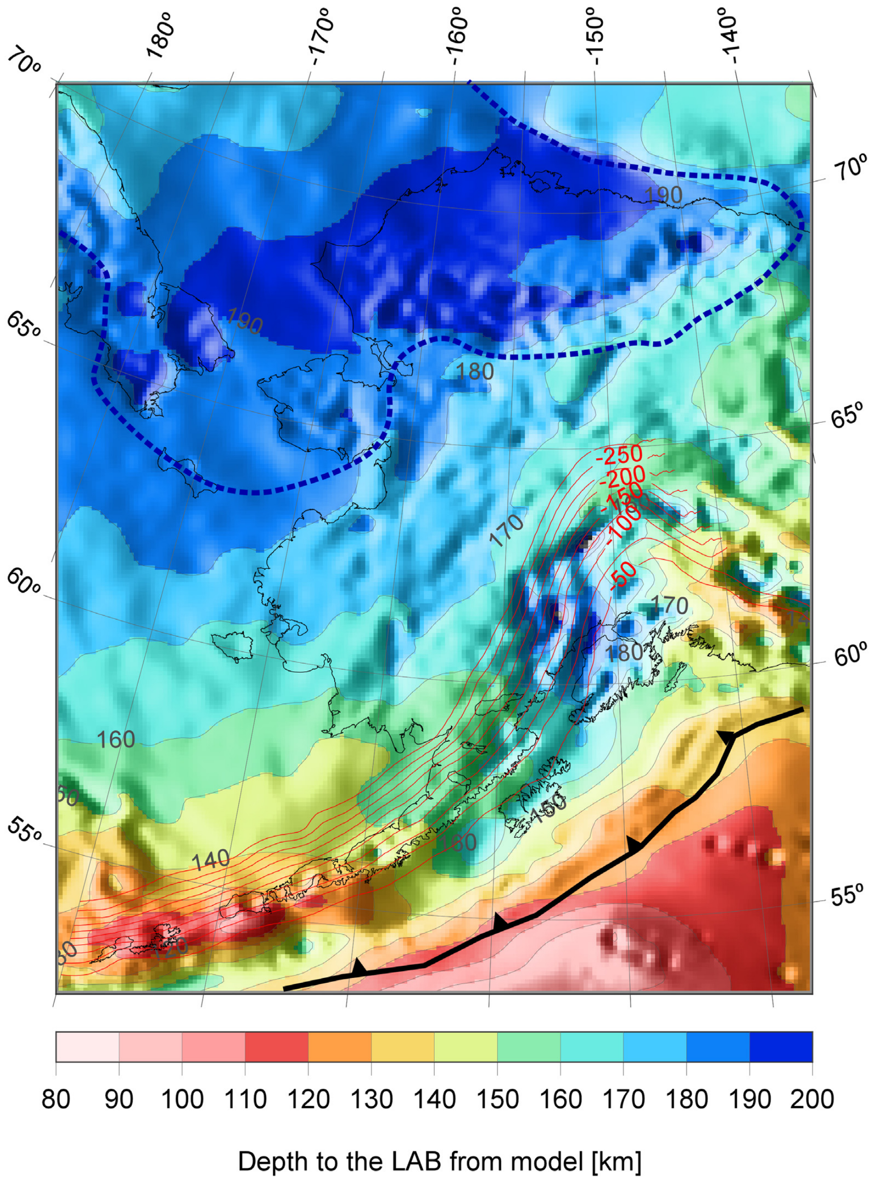

Figure 6. Depth to the LAB obtained from joint modelling elevation and geoid data, together with thermal analysis. Colour key shows depth to the LAB. Contours every 10 km. Dashed blue line shows position of Chukotka-Arctic Alaska microplate. Dark red contours show depth to top of the subducted plate (Model slabE115 of Jadamec & Billen 2010).

South of the Denali fault the LAB topography is complex, showing a local minimum (130–140 km) east of 150°W, below Wrangellia, Yakutat and the eastern side of the Chugach and Prince William terranes. The LAB increases to the west of 150°W, with larger values underneath the central areas of the Koyukuk, Peninsular and Chugach Terranes. The NW trending limit separating the thinner/hot lithosphere in the east and thick/colder lithosphere in the west (Fig. 6) coincides fairly well with observations.

4.3 Residual gravity field and density

The calculated residual gravity anomalies and the lateral average crustal density variations obtained from 3-D inversion of the model residual anomalies are shown in Figs 7(a) and (b), respectively. Fig. 7(a) shows wide regions with residual anomalies between –10 and 10 mGal, which are considered to fall within the resolution of this study. From this figure we also observe three main regions.

The northern region, north of 67°N, mainly characterized by the presence of mid-to-long wavelength negative residuals along the Chukchi and Beaufort shelves and north of the Brooks Range deformation front. This mid-to-long wavelength negative pattern contrasts with the presence of two positive anomalies along the shelf break and the short-wave length alternating positive and negative anomalies observed along the Brooks Range and Colville foredeep basin (Figs 2 and 7a). The central region covering the offshore Inner and Outer Bering shelves and central Alaska is broadly characterized by the presence of local positive and negative spots, particularly onshore. Southern Alaska, south of the Denali Fault, is characterized by nested arcuate positive anomalies that delineate

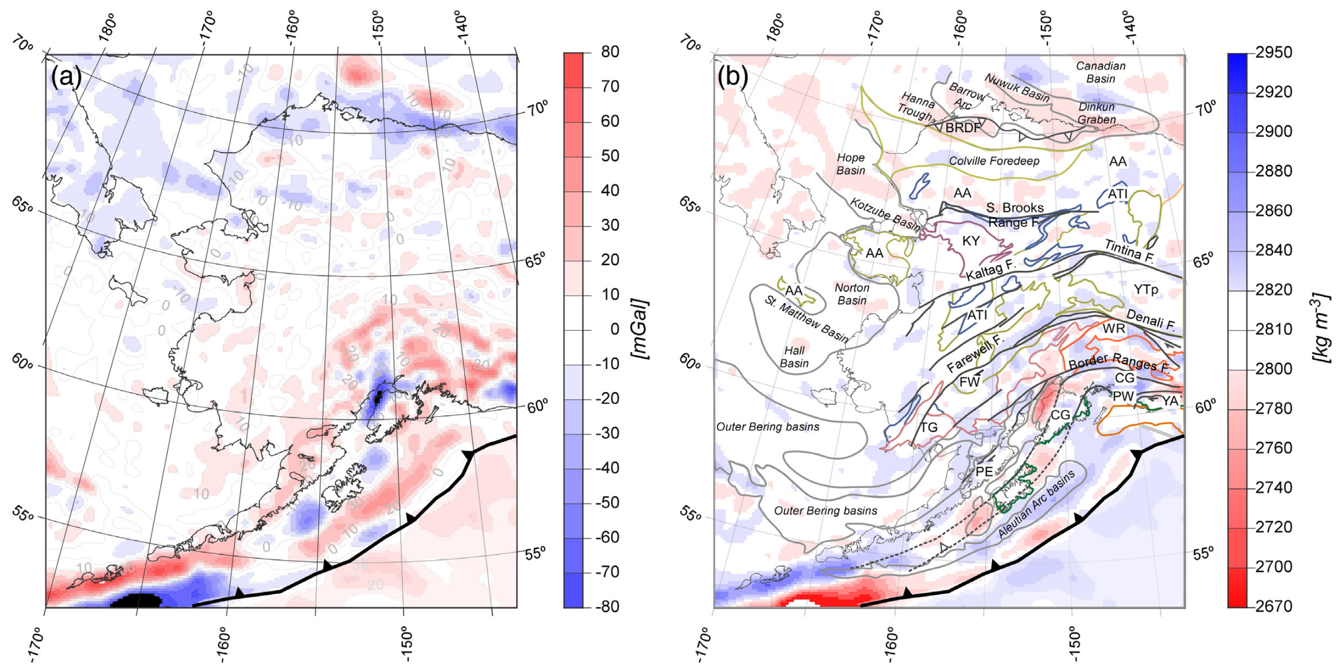

Figure 7. (a) Residual gravity anomaly map resulting from subtracting the regional gravity calculated from the lithospheric structure shown in Figs 5 and 6 to the measured one (Fig. 3b). (b) Lateral average crustal density variations calculated from residual gravity anomalies shown in panel (a). Contours every 10 kg m^{-3}. Superimposed main tectonic features and terranes. See Fig. 2 for legend.

the accreted Wrangellia Composite and the outboard Chugach terranes, interrupted by low density spots, the most noticeable being the low associated with the Cook Inlet basin.

Central and SW Alaska together with the Inner Bering Shelf are characterized by small short-wavelength positive and negative anomalies associated with local features, for which discussion is outside the scope of this study. At regional scales we may conclude that the average crustal density is close to 2810 kg m^{-3} (Fig. 7b).

South of the Denali Fault, there is an abrupt change of the residual anomaly pattern that does coincide with a change in the crustal structure observed for both surficial and deep levels (Fig. 5). Onshore, the high amplitude arcuate positive residual anomalies locally exceeding 60 mGal indicate the presence of a denser crust, related to Wrangellia, Peninsular and Chugach accreted terranes (Fig. 7b). The predicted gravity and density anomalies are described in the context of Alaska's history of terrane accretion and the resulting observed compositional variations in Section 5.3.

5 DISCUSSION

We now compare the modelled crustal thickness map and lithospheric structure obtained in this study to previous work and interpret the results in the context of Alaska's history of terrane accretion. In addition, we discuss the obtained residual gravity anomalies and the associated lateral average crustal density variations and relate them with the main terranes and geological features. Jointly analysing the structure of the crust and the lithospheric mantle of Alaska and of the adjacent Bering and Chukchi shelves can help to better understand the lithospheric geometry configured under a complex 200-Myr lasting long-term northward subduction of the Pacific Plate. The modelled crustal structure, under the different mountain ranges building Alaska, the attenuation of these mountain ranges to the west and the crustal geometry of the passage between the Brooks Range and its foreland system towards the Canadian basin are discussed below. The large-scale lithospheric structure beneath Alaska formed during the protracted Pacific Ocean subduction is an objective of this study, and the potential geodynamic implications inferred from the geometry of the LAB are described in this section as well.

5.1 Model limitations

The methodology used in this study is based on several assumptions that, in some places, might not apply entirely due to the complexity of the study region. In addition to the simplifications related to the densities of the crust and the lithospheric mantle, the strongest hypotheses are the prevalence of local isostasy, thermal steady-state regime and that the density of the lithospheric mantle is T-dependent. Local isostasy is a widely accepted approximation for wavelengths of tens to hundreds of kilometers depending on the effective elastic thickness and load distribution (e.g. Watts 2001; Turcotte & Schubert 2014). In our case, the possible flexure effects will be minor due to the filtered wavelengths of elevation and geoid data used. The assumption of thermal steady–state tends to overestimate or underestimate the lithospheric thicknesses in regions that have recently undergone thinning or thickening processes, respectively (Jiménez–Munt *et al.* 2011). This assumption is valid for most of north and central regions of the study area, but it is more difficult to ascertain in the southern margin affected by active subduction. Furthermore, the assumption that T increases with depth prevents us for modelling regions affected by inversion of temperature with depth, and therefore, to fully reproduce the current geometry of the subducting slab. Consequently, the LAB model presented in this work necessarily must be interpreted in terms of the physical conditions needed to produce the density distribution required to fit elevation and geoid anomalies rather than the current thermal boundaries (for a detailed discussion, see Fullea *et al.* 2007; Robert *et al.* 2015; Globig *et al.* 2016).

Although it is known that mantle density depends on the temperature, pressure and on composition, the used thermal approach has minor effects on the LAB geometry, since we do not calculate the actual density distribution of a given lithospheric column but the buoyancy relative to a given reference column, with known geometry, density, elevation and N_0 value. Previous studies in the Gibraltar-Arc region, where large variations in crust and lithospheric mantle thickness occur, corroborate that the differences in the calculated LAB depth are not significant when using a constant lithospheric mantle density, a pure thermal approach or a thermal and petrological approach (Fullea *et al.*, 2006, 2007, 2010).

5.2 Discussion of crustal structure in Alaska and adjacent shelves

Our results agree with the major regional crustal thickness trends registered by seismic data (e.g. Eberhart-Phillips *et al.* 2006; Veenstra *et al.* 2006; Fuis *et al.* 2008; O'Driscoll & Miller 2015), particularly with PRF of Miller & Moresi (2018) (Fig. 8). Most differences are within the range of ±3 to ±6 km, which are under the optimal error of DSS (Waldhauser *et al.* 1998) and RF seismic data (Spada *et al.* 2013). Moreover, we have also compared our results with the SRF Moho proposed by O'Driscoll & Miller (2015) and the PRF Moho of Miller & Moresi (2018) along four available profiles. Comparing the three datasets (Fig. 9) we observe that while there is generally a good agreement between PRF and our results along the selected profiles (see inset of Fig. 9 for location), major discrepancies arise with the SRF Moho. Overall, the SRF Moho is shallower for the majority of the profiles, particularly in south central Alaska. However, it should be noted that O'Driscoll & Miller (2015) provide the SRF–Moho picks as a first-order interpretation since the RF–Moho is better resolved by PRF studies.

Overall, the results here fit well with those from previous studies and expand the crustal thickness model to the offshore Chukchi and Bearing shelves. In northern Alaska, our results are consistent with results of Fuis *et al.* (2008); Miller *et al.* (2018) and Miller & Moresi (2018) that also find a thick crust beneath the Brook Ranges and the Colville foredeep basin, although locally there are some differences (Fig. 8). PRF record a thicker crust at a few stations located on the northern slope of the Brooks Range and at its westernmost end where the topography is smoother. Further to the north, in the Cretaceous Colville foredeep basin, we estimate a slightly thicker crust (2–4 km) when compared to the PRF results, but thinner compared to the results of the Trans–Alaska Transect (Fuis *et al.* 2008). These discrepancies may be explained by the presence of a lower crust characterized by average *P*-wave velocities of 7.8 km s^{-1}. These high velocities could partially mask our model results, for example the high density/velocity lower crust may be compensated by low density/velocity uppermost mantle and PRF results, for example the middle/lower crust being the main velocity contrast interface. In the central regions the thickness of the crust remains quite constant 34–36 km. This is probably related to the Middle Cretaceous extension and plutonism that according to Fuis *et al.* (2008) has left a uniform crust characterized by upper crustal velocities in the range of 6.0–6.4 km s^{-1}, a thin to absent lower crust, and a relative flat Moho.

The change in crustal thickness south of the Denali fault predicted by our study has been observed in previous works where large variations of Moho values occur over short distances (e.g. Eberhart-Phillips *et al.* 2006; Veenstra *et al.* 2006; Fuis *et al.* 2008; O'Driscoll & Miller 2015), likely due to the history of terrane accretion and variation in terrane composition and deformation history. The arcuate crustal structure observed at both surficial and deep levels is likely the result of transcurrent motion and oblique subduction along the NW North American margin. Thus, the sharp crustal thickness gradient across the Denali fault may be acting as a tectonic buttress or backstop facilitating an escape tectonics scenario in which the crustal curvature is guiding block motion west and south towards the subduction zone (Redfield *et al.* 2007; Jadamec *et al.* 2013; Haynie & Jadamec 2017).

In the southernmost region, the presence of multiple interfaces at both lithospheric mantle and crustal scale makes it difficult to identify the true seismic Moho. Furthermore, the presumable presence of a 'double Moho', the continental Moho of the overriding and the oceanic Moho of the subducting plate, adds some uncertainties to our results since our methodology does not allow for resolving a 'double Moho' structure. Offshore, there is no vestige of the continuation of the crustal pattern observed in mainland Alaska. Fig. 5 shows that the crust gently thickens in a S–N direction from 32 km in the southern Outer Bering shelf to 36 km in the northern areas of the Inner Bering shelf.

5.3 Discussion of LAB in Alaska region and adjacent shelves

Our modelling results show that northern Alaska and the Chukchi Shelf are characterized by the presence of a thick lithosphere (Fig. 6). Similar results have been reported in northern Alaska by Saltus & Hudson (2007) and O'Driscoll & Miller (2015) which can be interpreted as the presence of a cold, strong lithosphere. A cold, strong lithosphere is also supported by the low heat flow values (<60 mW m^{-2}) reported by Batir *et al.* (2016, Fig. 3a). Furthermore, Saltus & Hudson (2007) based on the presence of large deep–source magnetic highs (>200 nT) along the North Slope (the North Slope deep magnetic high–NSDMH) propose the presence of a voluminous mafic zone in the middle and lower crust that implies geochemical depletion of the upper mantle. These authors infer that the zone of magnetic highs is an indicator of strong lower crust and upper mantle that has acted as a buttress or tectonic backstop against compressional deformation that influences the current geometry of the Brooks Range fold-and-thrust belt (Moore *et al.* 1994, 1997) and southern areas.

The existence of this rigid backstop agrees with our results, with the LAB thermal structure constructed for 3-D numerical modelling of Alaska dynamics (Jadamec & Billen 2010; Jadamec *et al.* 2013) and with the conceptual 'escape tectonics' scenario of Redfield *et al.* (2007). The 3-D thermal structure used with thicker and stronger lithosphere in north Alaska resulted in the reproduction of the first-order tectonic deformation in Alaska (Jadamec *et al.* 2013; Haynie & Jadamec 2017). In the Redfield *et al.* (2007) conceptual model, the authors postulate that, since the Eocene, terranes have ascended along regional strike–slip faults from the British Columbia Margin to central Alaska, encountered a backstop, and escaped to the SW towards the Aleutian–Bering Sea subduction zones, through the so called North Pacific Rim Orogenic Stream (NPRS).

In the onshore central region, between the Southern Brooks Range extensional faults to the Denali-Farewell faults, the obtained thick lithosphere, from 160 to 180 km, is in disagreement with surface heat-flow estimates and with some interpretations of *S*-wave Receiver Function analysis. In a recent heat flow compilation, Batir

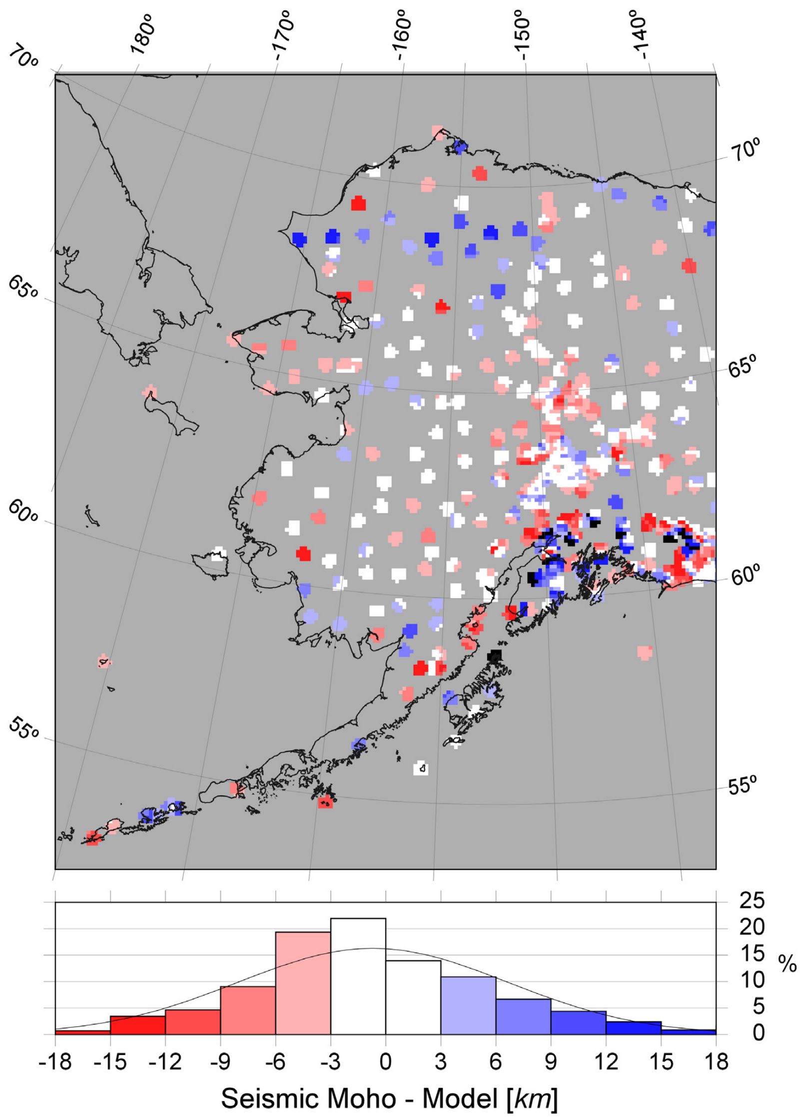

Figure 8. Differences between spot measurements of Moho depth estimates gathered from Ai *et al.* (2005), Miller & Moresi (2018), Miller *et al.* (2018) and Rossi *et al.* (2006) and our model results. Colour key shows differences at 3 km interval.

et al. (2016) suggest that much of interior Alaska, between the Alaska Range and the Brooks Range, may have values from 61 to 106 mWm^{-2}, with variations as high as 20 mWm^{-2} above and below the regional heat flow value. O'Driscoll & Miller (2015), based on *S*-wave receiver functions report the presence of two strong continuous field of negative conversions between 75–90 km and 140–150 km. Based on the surface heat flow results of Batir *et al.* (2016) they interpret the 75–90 km negative conversion as the LAB (e.g. YTU and YTT of Fig. 9, Profile C). These interpretations however, have some major caveats that allow us to give support to our results despite the mentioned discrepancies.

The heat flow map by Batir *et al.* (2016) in central Alaska is based on a very scarce and irregular distribution of thermal gradient measurements combined with the widespread presence of thermal springs, which induced the authors to propose a mantle derived origin for the high heat flow estimates. Nevertheless, the region affected by this high heat flow shows a low topography relative to the bounding Brook Range and the Alaska Range and is affected by deep faulting. These geological conditions are favorable for deep groundwater circulation generating positive regional thermal anomalies in the discharge area (e.g. Smith & Chapman 1983) and the presence of hot springs associated to deep master faults (Fernàndez and Banda 1990). On the other hand, a surface heat flow of 85 mW m^{-2} results in a lithospheric thickness of 74 km and an isostatic elevation of 1500 m by keeping a crustal thickness of 35 km, whereas the average elevation in the region is below 500 m (Figs 1 and 3). In addition, this shallow LAB would largely modify the geoid and the regional Bouguer gravity anomaly. Concerning to seismic data, O'Driscoll & Miller (2015) admit an alternative interpretation in which the shallow observed discontinuity corresponds to a MLD (mid lithospheric discontinuity), which would make the LAB deeper (unlabeled negative conversions seen in Fig. 9, Profile C) in agreement with our results.

South of the Denali Fault, interpreting the predicted LAB becomes complicated by the flat slab beneath south central Alaska associated with subduction of the Pacific Plate and Yakutat plateau. A subducted slab shape that extends to a shallower depth beneath the Wrangell mountains and to a deeper depth to the west is consistent with previous studies (Page *et al.* 1989; Ratchkovski & Hansen 2002; Jadamec & Billen 2010; Wang & Tape 2014; Chuang

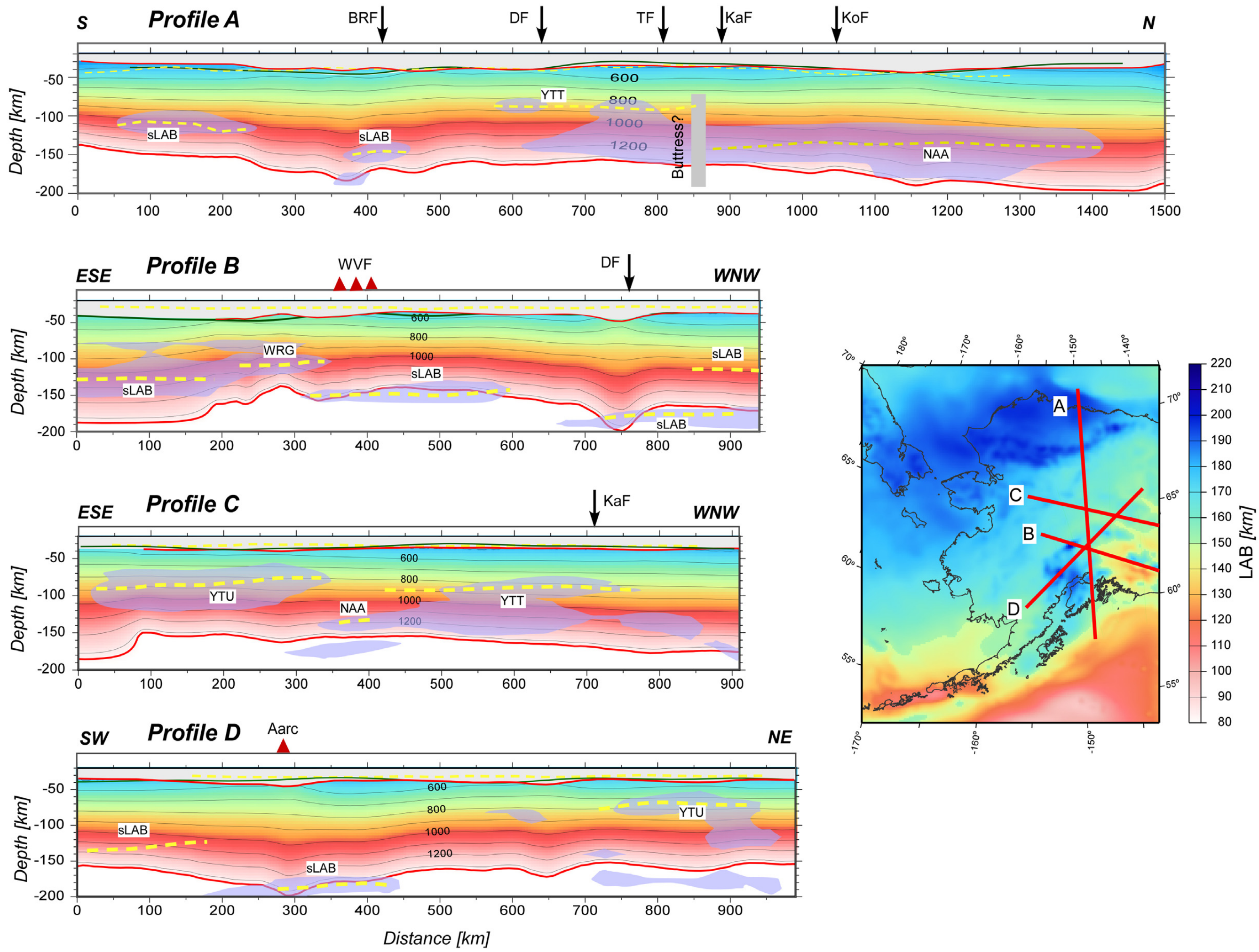

Figure 9. Comparison of Moho and LAB depths obtained in this study to those obtained from RF data. (a) Location of compared cross sections. (b) Results from our study are: Temperature (colour palette), Moho (red line) and LAB depth (thick red line). Results from previous studies and different methodologies: PRF Moho of Miller *et al.* (2018) and Miller & Moresi (2018) (green line). SRF Moho of O'Driscoll & Miller (2015) (Yellow thin dashed line). SRF LAB of O'Driscoll & Miller (2015) (Yellow thick dashed line). Grey box of profile A indicates the lithospheric buttress proposed by O'Driscoll & Miller (2015). Light grey shaded areas show the crust from this study. Blue light shaded areas show areas of SRF negative conversions that arise from slow-to-fast velocity interfaces, possible LABs (digitized from O'Driscoll & Miller 2015). Red triangles show the location of Quaternary volcanoes. Volcanic fields: WVF–Wrangell and Arc–Aleutian. Faults: BRF–Border Ranges, DF–Denali, KaF–Kaltag, KoF–Kobuk, TF–Tintina. Terranes: YTT–Yukon–Tanana Terrane, YTU–Yukon–Tanana Upland, NAA–North Alaska Arctic. sLAB–slab LAB. See Fig. 2 for legend.

et al. 2017). Beneath the Wrangell volcanoes, the Pacific Plate only extends to ~100 km, suggesting that there is no vestige of the Yakutat terrane protruding into the mantle beneath the Wrangell mountains, and that this region is already underplated beneath the St. Elias Range (Eberhart-Phillips *et al.* 2006; Jadamec & Billen 2010; Fuis *et al.* 2008. Beneath south central Alaska, both the Pacific oceanic lithosphere and the Yakutat terrane subduct together forming a northwestward directed flat slab at shallow depths (Eberhart-Phillips *et al.* 2006, Fuis *et al.* 2008; Jadamec & Billen 2010). Farther west, the slab resumes a more typical slab dip (Jadamec *et al.* 2018).

Based on the 400 km gap of volcanism and slab seismicity observed between the Aleutian arc and the Wrangell volcanics, Fuis *et al.* (2008) infer the presence of a slab tear in the subducting Pacific Plate beneath south central Alaska (see their Fig. 7 in Plate 1). Alternatively, a comprehensive slab shape for the region based on the synthesis of over 10 seismic studies, suggests the slab is continuous at shallow depths, but forms two-tiered shape at depth, with a shorter slab segment beneath the Wrangells (SlabE115 in Jadamec & Billen 2010, 2012). This suggests there is not a tear in the sense of a slab window, but rather that the deeper segment of the eastern Wrangell slab is missing, possibly due to slab detachment. Thus, the SlabE115 shape explains the observations without the need for an intraslab tear (Jadamec & Billen 2010, 2012; Wang & Tape 2014). 3-D geodynamic models of Alaska that incorporate the two-tiered slab shape produce warm mantle upwellings adjacent to the slab beneath the Wrangell volcanics, providing a geodynamic mechanism for the anomalous volcanism and possibly thinned lithosphere in this region (Jadamec & Billen 2010; Jadamec & Billen 2012; Jadamec 2016a). This is consistent with the global *P*-wave tomography model of Simmons *et al.* (2012). Fig. 10 shows that east of 150°W and south of 62°N there is no vestige of positive anomalies, whereas to the west the positive anomaly extends down to 220 km depth.

Fig. 9 shows comparison of our resulting thermal LAB with the SRF results of O'Driscoll & Miller (2015) along four selected profiles that cross the eastern regions of central and southern Alaska

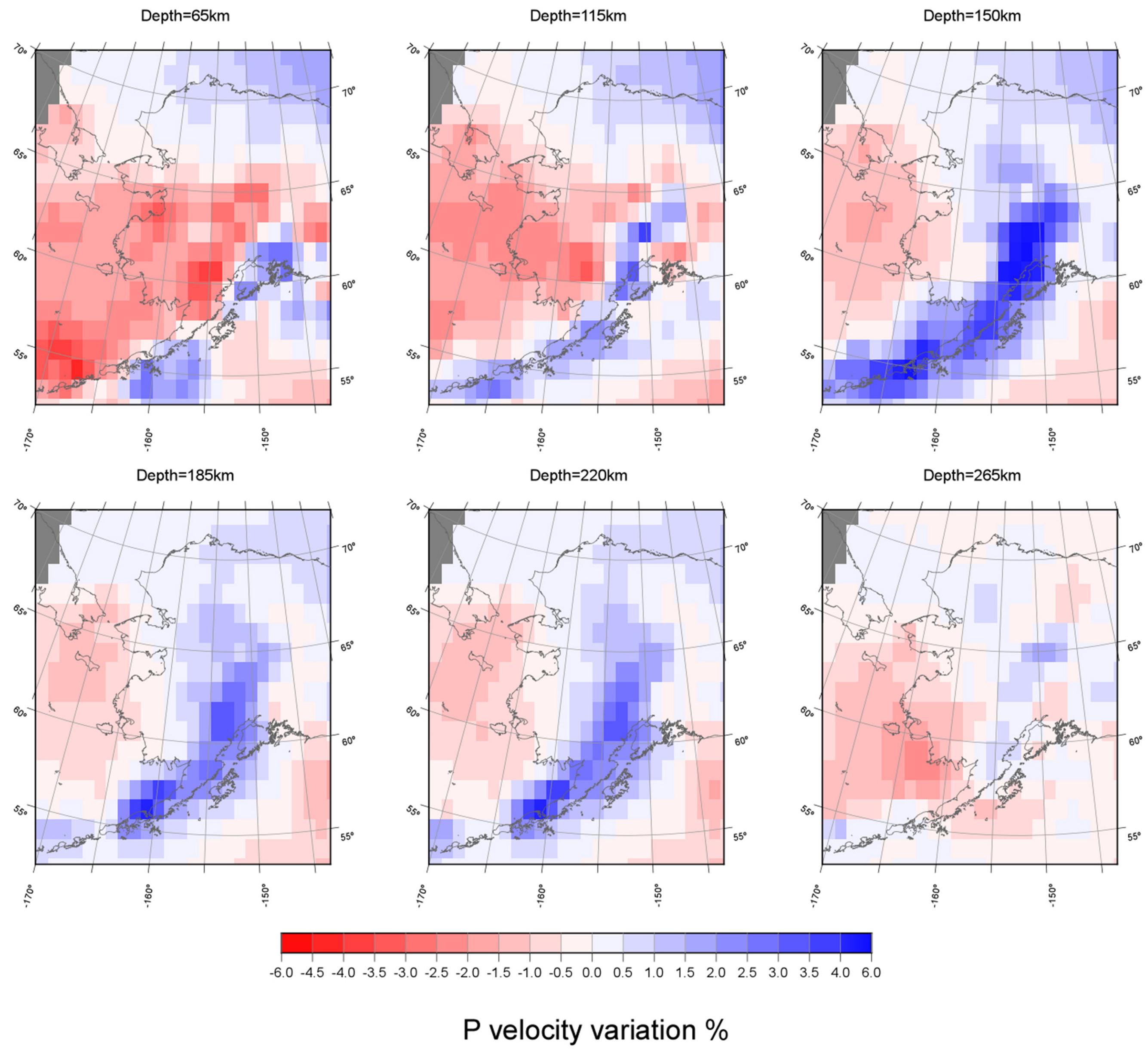

Figure 10. *P* velocity variations at different depths from tomographic model of Simmons *et al.* (2012).

(inset of Fig. 9a). We observe that there is coincidence in 1) a lithospheric thickening towards the north, from the active orogeny and back arc areas to the stable interior (where the LAB reaches values above 150 km), and 2) overall with respect to the depth where the LAB of the subducting plate (sLAB) is found in central Alaska (Fig. 9). Our predicted LAB coincides with the sLAB depth along the majority of profiles (Profiles B and D of Fig. 9) with the exception of the southernmost areas, for example south of the Border Ranges Fault and around the Aleutian Arc where our model fails to precisely predict the location of the LAB (see above). Furthermore, SRF results also image a lithospheric thinning underneath the Wrangell volcanic field and thickening west of 150°W (Profile B of Fig. 9). Comparison with SRF results in Western Alaska and along the western shelves is more complex since, according to O'Driscoll & Miller (2015), the wide station spacing results in each station averaging structures across a wide spatial domain of ∼150 km radius, thus being biased towards the dominant event source locations.

5.4 Discussion of residual gravity field and density

Offshore northern and western Alaska, negative residuals along the Chukchi Shelf broadly delineate the South Chukchi (Hope) Basin filled by Cenozoic non-marine, marine, and lacustrine rocks with sediment thickness in the range of 3–4 km and locally up to 5–6 km (Verzhbitsky *et al.* 2008). Along the Beaufort Shelf, negative anomalies coincide with the Nuwuk–Dinkum–Kaktovik basin where sediment accumulations exceeding 5 km are registered (Figs 2 and 7).

More difficult to correlate with surficial geology are two positive residual anomalies (>50 mGal) north of 70°N following the trend of the continental shelf break (Fig. 7a). Free-Air gravity elongated highs with pronounced gradients and values above 50 mGal are observed all along the continental shelf break of the eastern and southern Canadian Basin (Helwig *et al.* 2011), as also reported at many other passive margins. As already pointed out by previous authors (e.g. Scrutton 1982), the Free-Air gravity highs are produced by the combination of two factors: (1) the edge effect associated with crustal thinning from the continental to the oceanic domain and (2) the presence of either a basement high or a high density zone along the outer shelf break. Our preference is that both highs are associated with a basement ridge at the outer shelf, since to our knowledge there is no evidence of high density material (e.g. uppermost mantle rocks) being emplaced at lower crustal levels.

Onshore, south of the Bering Strait, Klemperer *et al.* (2002) and Miller *et al.* (2017), both based on deep seismic reflection profiling, report a relatively thick crystalline crust with the basement located at or near the surface. According to these authors, the upper crust is characterized by broad basement arcs with thin intervening Neogene sedimentary basins, for example the Norton and St. Matthew and Hall basins where sediment accumulations are less than 3 km (Fig. 2). The middle crust is characterized by Early Cretaceous to Palaeogene plutons while the lower crust is underplated by Early Cretaceous to Palaeogene gabbroic intrusives and mafic sills, younging from north to south. Thus, the presence of a thick crystalline crust with underplated material explains the slight increase of the average density of the crust compared to the northern region—as predicted by our lithospheric model.

In south central Alaska, north of the Border Ranges Fault, the predicted crustal densification may be related to the oceanic nature of the Wrangellia Composite terrane rocks. In Alaska, that terrane is mainly composed of variably metamorphic mafic to intermediate arc-related volcanic rocks of Palaeozoic age overlaid by a thick pile (up to 6000 m thick) of Middle-to-Late Triassic flood basalts and Upper Triassic to Lower Jurassic shallow marine silicic and calcareous rocks (Plafker & Berg 1994). South of the Border Ranges Fault, the Chugach Terrane is a complexly deformed accretionary prism formed by Upper Triassic to Palaeogene oceanic rocks and dominantly arc-related volcanic and volcanoclastic rocks off-scraped from the subducting Pacific Plate (Plafker & Berg 1994). Among the residual gravity highs there is a prominent NE residual low associated with the thick sedimentary rocks of the Cook Inlet basin. 3-D geodynamic modelling of Alaska predicts localized but significant negative dynamic topography in the Cook Inlet basin, where the upper plate lithosphere is dynamically depressed, providing a geodynamic mechanism for the sediment infill (Jadamec *et al.* 2013).

6 CONCLUSIONS

This study presents for the first time an integrated image of the crust and lithospheric mantle of Alaska and its adjacent western shelves of the Chukchi and Bering seas based on joint modelling of potential field data and thermal analysis constrained by seismic data.

Our results show a long wavelength northwest directed crustal thickening (32–36 km) superimposed over onshore Alaska with two local crustal thickening trends that broadly correlate with topography. Crustal thicknesses above 40 and 50 km are found in the northern Brooks Range and in the Alaska and St Elias ranges, respectively

The sharp crustal thickness gradient along the Denali Fault agrees with the presence of a crustal tectonic buttress that would facilitate an 'escape tectonics' scenario in which the crustal curvature is guiding block motion west and south towards the subduction zone. Offshore, north of St Lawrence Island we observe a slightly anomalous thick crust relative to the shallow bathymetry of the area, gently thickening towards the Chukchi Shelf.

The denser crust, up to 2910 kg m^{-3}, is found south of the Denali Fault likely related to the oceanic nature of the Wrangellia Composite Terrane rocks and the high *P*-wave velocity recorded at mid-lower crustal levels below the Chugach Terrane. Some low-density anomalies are interspersed, highlighting the low associated with the forearc Cook Inlet Basin. Offshore, less dense crust (below 2780–2800 kg m^{-3}) is found along the Chukchi and Beaufort shelves, which relates to the sedimentary infill of the South Chukchi (Hope) and Nuwuk–Dinkum–Kaktovik basins, respectively. The two high density anomalies (above 2860 kg m^{-3}) following the trend of the Beaufort continental shelf break are likely related to the presence of a basement ridge on the outer shelf. However, we cannot rule out that the density increase is also related to high density rocks emplaced at mid-to-lower crust levels (e.g. uppermost mantle rocks).

At LAB levels, there is a regional SE–NW trend that coincides with the current motion of the subducting Pacific Plate with a lithospheric root underneath the Brooks Range, Northern Slope and Chuckchi Sea, that may correspond to a relic of the Chukotka-Artic Alaska microplate. The obtained lithospheric root (above 180 km) agrees with the presence of a boundary of cold, strong lithosphere that deflects the strain towards the South, thus influencing the current geometry of the Brooks Range belt and the southern regions. South of the Denali Fault the LAB topography is quite complex. East of 150°W, below Wrangellia and the eastern side of Chugach terranes the LAB is much shallower than it is west of this meridian. The NW trending limit separating the thinner lithosphere in the east and thick lithosphere in the west agrees with the two-tiered slab shape of the subducting Pacific Plate and with tomographic data.

ACKNOWLEDGEMENTS

This research has been funded by the We–Me project (PIE–CSIC–201330E111), AGAUR 2017–SGR–847, Alpimed (PIE-CSIC-201530E082), Subtetis (PIE-CSIC-201830E039) and funds from the University of Houston. We deeply acknowledge Meghan S. Miller and Louis Moresi for giving us access to PRF data that have greatly contributed to constraining the presented 3-D lithospheric model. We are indebted to Drs. Holzrichter, Paulatto and Petit who provided interesting and helpful comments and suggestions that helped us improve the original version of the manuscript. Figs 1–10 were totally or partly drawn using GMT software (Wessel *et al.* 2013).

REFERENCES

Ai, Y., Zhao, D., Gao, X. & Xu, W., 2005. The crust and upper mantle discontinuity structure beneath Alaska inferred from receiver functions, *Phys. Earth planet. Inter.,* **150**(4), 339–350.

Artemieva, I.M., 2006. Global 1× 1 thermal model TC1 for the continental lithosphere: implications for lithosphere secular evolution, *Tectonophysics,* **416**(1), 245–277.

Artemieva, I.M. & Mooney, W.D., 2001. Thermal thickness and evolution of Precambrian lithosphere: a global study, *J. geophys. Res.,* **106**(B8), 16 387–16 414.

Bassin, C., 2000. The current limits of resolution for surface wave tomography in north America, *EOS, Trans. Am. geophys. Un.,* **81**(48), F897, Fall Meet. Suppl., Abstract S12A–03.

Batir, J.F., Blackwell, D.D. & Richards, M.C., 2016. Heat Flow and temperature-depth curves throughout Alaska: finding regions for future hydrothermal explorations, *J. Geophys. Eng.,* **13,** 366–377.

Bird, P., 1996. Computer simulations of Alaskan neotectonics, *Tectonics,* **15**(2), 225–236.

Bruns, T.R., 1983. Model for the origin of the Yakutat block, an accreting terrane in the northern Gulf of Alaska, *Geology,* **11**(12), 718–721.

Carballo, A., Fernandez, M., Torne, M., Jiménez-Munt, I. & Villaseñor, A., 2015a. Thermal and petrophysical characterization of the lithospheric mantle along the northeastern Iberia geo-transect, *Gondwana Res.,* **27**(4), 1430–1445.

Carballo, A. *et al.*, 2015b. From the North-Iberian Margin to the Alboran Basin: a lithosphere geo-transect across the Iberian Plate, *Tectonophysics,* **663,** 399–418.

Christeson, G.L., van Avendonk, H.J., Gulick, S.P.S., Reece, R.S., Pavlis, G.L. & Pavlis, T.L., 2013. Moho interface beneath Yakutat terrane, southern Alaska, *J. geophys. Res.,* **118,** 5084–5097.

Chuang, L., Bostock, M., Wech, A. & Plourde, A., 2017. Plateau subduction, intraslab seismicity, and the Denali (Alaska) volcanic gap, *Geology,* **45**(7), 647–650.

Coney, P.J. & Jones, D.L., 1985. Accretion tectonics and crustal structure in Alaska, *Tectonophysics,* **119,** 265–283.

Conrad, C.P., Behn, M.D. & Silver, P.G., 2007. Global mantle flow and the development of seismic anisotropy: differences between the oceanic and continental upper mantle, *J. geophys. Res.,* **112**(B7).

Daradich, A., Mitrovica, J.X., Pysklywec, R.N., Willett, S.D. & Forte, A.M., 2003. Mantle flow, dynamic topography, and rift-flank uplift of Arabia, *Geology,* **31**(10), 901–904.

Eaton, D.W., Darbyshire, F., Evans, R.L., Grütter, H., Jones, A.G. & Yuan, X., 2009. The elusive lithosphere–asthenosphere boundary (LAB) beneath cratons, *Lithos,* **109**(1-2), 1–22.

Eberhart–Phillips, D., Christensen, D.H., Brocher, T.M., Hansen, R., Ruppert, N.A., Haeussler, P.J. & Abers, G.A., 2006. Imaging the transition from Aleutian subduction to Yakutat collision in central Alaska, with local earthquakes and active source data, *J. geophys. Res.,* **111,** B11303.

Enkelmann, E., Zeitler, P.K., Pavlis, T.L., Garver, J.I. & Ridgway, K.D., 2009. Intense localized rock uplift and erosion in the St. Elias orogen of Alaska, *Nat. Geosci.,* **2**(5), 360.

Fernández, M. & Banda, E., 1990. Geothermal anomalies in the Valles-Penedes graben master fault: convection through the horst as a possible mechanism, *J. geophys, Res.,* **95**(B4), 4887–4894.

Ferris, A., Abers, G.A., Christensen, D.H. & Veenstra, E., 2003. High resolution image of the subducted Pacific (?) plate beneath central Alaska, 50–150 km depth, *Earth planet. Sci. Lett.,* **214,** 575–588.

Fischer, K.M., Ford, H.A., Abt, D.L. & Rychert, C.A., 2010. The lithosphere-asthenosphere boundary, *Annu. Rev. Earth Planet. Sci.,* **38,** 551–575.

Fitzgerald, P.G., Sorkhabi, R.B., Redfield, T.F. & Stump, E., 1995. Uplift and denudation of the central Alaska Range: a case study in the use of apatite fission track thermochronology to determine absolute uplift parameters, *J. geophys. Res.,* **100**(B10), 20 175–20 191.

Flament, N., Gurnis, M. & Müller, R.D., 2013. A review of observations and models of dynamic topography, *Lithosphere,* **5**(2), 189–210.

Fuis, G., Murphy, J., Lutter, W., Moore, T., Bird, K. & Christensen, N., 1997. Deep seismic structure and tectonics of northern Alaska: crustal–scale duplexing with deformation extending into the upper mantle, *J. geophys. Res.,* **102**(B9), 20 873–20 896.

Fuis, G.S. *et al.*, 2008. Trans–Alaska Crustal Transect and continental evolution involving subduction underplating and synchronous foreland thrusting, *Geology,* **36**(3), 267–270.

Fullea, J., Afonso, J.C., Connolly, JAD, Fernàndez, M., García-Castellanos, D. & Zeyen, H., 2009. LitMod3D: An interactive 3-D software to model the thermal, compositional, density, seismological, and rheological structure of the lithosphere and sublithospheric upper mantle, *Geochem., Geophys., Geosyst.,* **10**(8).

Fullea, J., Fernàndez, M., Afonso, J.C., Vergés, J. & Zeyen, H., 2010. The structure and evolution of the lithosphere–asthenosphere boundary beneath the Atlantic–Mediterranean Transition Region, *Lithos,* **120**(1-2), 74–95.

Fullea, J., Fernàndez, M. & Zeyen, H., 2006. Lithospheric structure in the Atlantic–Mediterranean transition zone, *C.R. Geosci.,* **338**(1-2), 140–151.

Fullea, J., Fernàndez, M. & Zeyen, H., 2008. FA2BOUG—a FORTRAN 90 code to compute Bouguer gravity anomalies from gridded free–air anomalies: application to the Atlantic–Mediterranean transition zone, *Comput. Geosci.,* **34**(12), 1665–1681.

Fullea, J., Fernàndez, M., Zeyen, H. & Vergés, J., 2007. A rapid method to map the crustal and lithospheric thickness using elevation, geoid anomaly and thermal analysis. application to the Gibraltar arc system, Atlas Mountains and adjacent zones, *Tectonophysics,* **430**(1), 97–117.

Fullea, J., Muller, M.R., Jones, A.G. & Afonso, J.C., 2014. The lithosphere–asthenosphere system beneath Ireland from integrated geophysical–petrological modeling II: 3D thermal and compositional structure, *Lithos,* **189,** 49–64.

Gallardo-Delgado, L.A., Pérez-Flores, M.A. & Gómez-Treviño, E., 2003. A versatile algorithm for joint 3D inversion of gravity and magnetic data, *Geophysics,* **68,** 949–959.

Gilardoni, M., Reguzzoni, M. & Sampietro, D., 2016. GECO: a global gravity model by locally combinig GOCE data and EGM2008, *Studia Geophysica et Geodaetica,* **60**(2), 228–247.

Globig, J., Fernàndez, M., Torne, M., Vergés, J., Robert, A. & Faccenna, C., 2016. New insights into the crust and lithospheric mantle structure of Africa from elevation, geoid, and thermal analysis, *J. geophys. Res.,* **121**(7), 5389–5424.

Greninger, M.L., Klemperer, S.L. & Nokleberg, W.J., 1999. Geographic Information Sys- tems (GIS) compilation of geophysical, geologic, and tectonic data for the circum-North Pacific, *Open-File Report 99–422*. United States Geological Survey.

Haxby, W.F. & Turcotte, D.L., 1978. On isostatic geoid anomalies, *J. geophys. Res.,* **83**(B11), 5473–5478.

Hayes, G.P., Moore, G.L., Portner, D.E., Hearne, M., Flamme, H., Furtney, M. & Smoczyk, G.M., 2018. Slab2, a comprehensive subduction zone geometry model, *Science,* **362**(6410), 58–61.

Haynie, K.L. & Jadamec, M.A., 2017. Tectonic drivers of the Wrangell block: Insights on forearc sliver processes from 3D geodynamic models of Alaska, *Tectonics,* **36,** 1180–1206.

Helwig, J., Kumar, N., Emmet, P. & Dinkelman, M.G., 2011. Regional seismic interpretation of crustal framework, Canadian Arctic passive margin, Beaufort Sea, with comments on petroleum potential, in *Arctic Petroleum Geology,* pp. 527–543. eds Spencer, A.M. Embry, A.F. Stoupakova, A.V. & Sorensen, K., Geological Society, London, Memoirs, **35**.

Herzberg, C. & Rudnick, R., 2012. Formation of cratonic lithosphere: an integrated thermal and petrological model, *Lithos,* **149,** 4–15.

Hopper, E., Ford, H.A., Fischer, K.M., Lekic, V. & Fouch, M.J., 2014. The lithosphere–asthenosphere boundary and the tectonic and magmatic history of the northwestern United States, *Earth planet. Sci. Lett.,* **402,** 69–81.

Jadamec, M.A., 2016a. Insights on slab-driven mantle flow from advances in three-dimensional modelling, *J. Geodyn.,* **100,** 51–70.

Jadamec, M.A., 2016b. Slab-driven mantle weakening and rapid mantle flow, *Subduction Dynamics: From Mantle Flow to Mega Disasters,* **211,** 135.

Jadamec, M.A. & Billen, M.I., 2010. Reconciling surface plate motions with rapid three-dimensional mantle flow around a slab edge, *Nature,* **465**(7296), 338–342.

Jadamec, M.A. & Billen, M.I., 2012. The role of rheology and slab shape on rapid mantle flow: three–dimensional numerical models of the Alaska slab edge, *J. geophys. Res.,* **117**(B02304), 20.

Jadamec, M.A., Billen, M.I. & Roeske, S.M., 2013. Three–dimensional numerical models of flat slab subduction and the Denali fault driving deformation in south–central Alaska, *Earth planet. Sci. Lett.,* **376,** 29–42.

Jadamec, M.A., Kreylos, O., Chang, B., Fischer, K.M. & Yikilmaz, M.B., 2018. A visual survey of global slab geometries with show Earth model and implications for a three-dimensional subduction paradigm, *Earth Space Sci.,* **5**(6), 240–257.

Jiménez-Munt, I., Fernández, M., Vergés, J., Garcia-Castellanos, D., Fullea, J., Pérez-Gussinyé, M. & Afonso, J.C., 2011. Decoupled crust–mantle accommodation of Africa–Eurasia convergence in the NW Moroccan margin, *J. geophys. Res.,* **116**(B8), B08403.

Jiménez–Munt, I., Fernàndez, M., Saura, E., Vergés, J. & García–Castellanos, D., 2012. 3–D lithospheric structure and regional/residual Bouguer anomalies in the Arabia–Eurasia collision, Iran), *Geophys. J. Int.,* **190**(3), 1311–1324.

Jones, A.G., Afonso, J.C., Fullea, J. & Salajegheh, F., 2014. The lithosphere–asthenosphere system beneath Ireland from integrated geophysical–petrological modeling—I: observations, 1D and 2D hypothesis testing and modeling, *Lithos,* **189,** 28–48.

Jones, D.L., Silberling, N.J., Berg, H.C. & Plafker, G., 1981. Tectonostratigraphic terrane map of Alaska: U.S. Geological Survey Open File Rept. 81–792, map, expl. sheet, and 20p.

Kalbas, J.L., Freed, A.M. & Ridgway, K.D., 2008. Contemporary fault mechanics in southern Alaska, *Active Tectonics and Seismic Potential of Alaska,* Geophysical Monograph Series 179, pp. 321–336, eds Freymueller J.T., Haeussler P.J., Wesson R.L. & Ekström G..

King, S.D. & Ritsema, J., 2000. African hot spot volcanism: small-scale convection in the upper mantle beneath cratons, *Science,* **290**(5494), 1137–1140.

Kirschner, C.E., 1992. Map showing sedimentary basins in Alaska. Plate 7. Sedimentary basins in Alaska, The Geology of Alaska, G1 of the Geology of North America.

Klemperer, S.L., Miller, E.L., Grantz, A. & Scholl, D.W., & the Bering–Chukchi Working Group, 2002. Crustal structure of the Bering and Chukchi shelves: deep seismic reflection profiles across the North American continent between Alaska and Russia, in *Tectonic Evolution of the Bering Shelf–Chukchi Sea–Arctic Margin and Adjacent Landmasses,* pp. 1–24. eds Miller, E.L. Grantz, A. & Klemperer, S.L.. Geological Society of America Special Paper **360**.

Lachenbruch, A.H. & Morgan, P., 1990. Continental extension, magmatism and elevation; formal relations and rules of thumb, *Tectonophysics,* **174**(1), 39–62.

Lee, C.T.A., 2003. Compositional variation of density and seismic velocities in natural peridotites at STP conditions: implications for seismic imaging of compositional heterogeneities in the upper mantle, *J. geophys. Res.,* **108**(B9).

Lekic, V. & Romanowicz, B., 2011. Tectonic regionalization without a priori information: a cluster analysis of upper mantle tomography, *Earth planet. Sci. Lett.,* **308**(1-2), 151–160.

Lewis, T.J., Hyndman, R.D. & Fluck, P., 2003. Heat flow, heat generation, and crustal temperatures in the northern Canadian cordillera: thermal controls of tectonics, *J. geophys. Res.*. **108**(B6), 2316.

Liu, M., Cui, X. & Liu, F., 2004. Cenozoic rifting and volcanism in eastern China: a mantle dynamic link to the Indo–Asian collision?, *Tectonophysics,* **393**(1-4), 29–42.

MacDougall, J.G., Jadamec, M.A. & Fischer, K.M., 2017. The zone of influence of the subducting slab in the asthenospheric mantle, *J. geophys. Res.,* **122**(8), 6599–6624.

Miller, E.L. *et al.*, 2017. Circum–Arctic Lithosphere Evolution (CALE) Transect C: displacement of the Arctic Alaska–Chukotka microplate towards the Pacific during opening of the Amerasia Basin of the Arctic, in *Circum–Arctic Lithosphere Evolution,* eds Pease, V. & Coakley, B., Geological Society, London, Special Publications, **460**.

Miller, M.S. & Moresi, L., 2018. Mapping the Alaskan Moho, *Seismol. Res. Lett.,* **89**(6), 2430–2436.

Miller, M.S., O'Driscoll, L.J., Porritt, R.W. & Roeske, S.M., 2018. Multiscale crustal architecture of Alaska inferred from P receiver functions, *Lithosphere,* **10**(2), 267–278.

Molnar, P., Houseman, G.A. & Conrad, C.P., 1998. Rayleigh—Taylor instability and convective thinning of mechanically thickened lithosphere: effects of non-linear viscosity decreasing exponentially with depth and of horizontal shortening of the layer, *Geophys. J. Int.,* **133**(3), 568–584.

Moore, T.E. & Box, S.E., 2016. Age, distribution and style of deformation in Alaska north 60° N: implications for assembly of Alaska, *Tectonophysics,* **691,** 133–170.

Moore, T.E., Wallace, W.K., Bird, K.J., Karl, S.M., Mull, C.G. & Dillon, J.T., 1994, *Geology of northern Alaska*.

Moore, T.E., Wallace, W.K., Mull, C.G., Adams, K.E., Plafker, G. & Nokleberg, W.J., 1997. Crustal implications of bedrock geology along the Trans-Alaska Crustal Transect (TACT) in the Brooks Range, northern Alaska, *J. geophys. Res.,* **102**(B9), 20 645–20 684.

Nokleberg, W.J., 2000. Phanerozoic tectonic evolution of the Circum–North Pacific, 1626, US Department of the Interior. US Geological Survey.

Nokleberg, W.J. *et al.*, 1994. *Circum-North Pacific Tectonostratigraphic Terrane Map (94-714)*. US Geological Survey.

O'Driscoll, L.J. & Miller, M.S., 2015. Lithospheric discontinuity structure in Alaska, thickness variations determined by S receiver functions, *Tectonics,* **34**(4), 694–714.

Page, R.A., Stephens, C.D. & Lahr, J.C., 1989. Seismicity of the Wrangell and Aleutian Wadati-Benioff zones and the North American plate along the Trans-Alaska crustal transect, Chugach Mountains and Copper River basin, southern Alaska, *J. geophys. Res.,* **94**(B11), 16 059–16 082.

Pavlis, T.L., Picornell, C. & Serpa, L., 2004. Tectonic processes during oblique collision: insights from the St. Elias orogeny, northern North American Cordillera, *Tectonics,* **23**.

Plafker, G. & Berg, H.C., 1994. Overview of the geology and tectonic evolution of Alaska, in *The Geology of Alaska: Boulder, Colorado,* eds Plakfer, G. & , Berg, H.C., Geological Society of America, The Geology of North America, **G-1,** 1068pp.

Plafker, G., Gilpin, L.M. & Lahr, J.C., 1994. Neotectonic map of Alaska, scale 1: 2,500,000. *Geology of Alaska, Map, GNA-G-1, Plate 12a*. The Geology of Alaska: Boulder, Colorado, *Geological Society of America*, The Geology of North America, G-1. 1068 pp.

Popowski, T., Connard, G. & French, R., 2005. *GMSYS–3D User Guide*. Northwest Geophysical Associates, Inc., 32pp.

Ratchkovski, N.A. & Hansen, R.A., 2002. New evidence for segmentation of the Alaska subduction zone, *Bull. seism. Soc. Am.,* **92**(5), 1754–1765.

Redfield, T.F., Scholl, D.W., Fitzgerald, P.G. & Beck, M.E., 2007. Escape tectonics and the extrusion of Alaska: past, present, and future, *Geology,* **35**(11), 1039–1042.

Robert, A.M., Fernàndez, M., Jiménez–Munt, I. & Vergés, J., 2015. Lithospheric structure in central Eurasia derived from elevation, geoid anomaly and thermal analysis, *Geol. Soc., Lond., Spec. Publ.,* **427,** SP427–10.

Root, B., Wal, W., Novák, P., Ebbing, J. & Vermeersen, L., 2015. Glacial isostatic adjusts in the static gravity field of Fennoscandia, *J. geophys. Res.,* **120**(1), 503–518.

Rossi, G., Abers, G.A., Rondenay, S. & Christensen, D.H., 2006. Unusual mantle Poisson's ratio, subduction and crustal structure in central Alaska, *J. geophys. Res.,* **111**(B9).

Rudnick, R.L. & Fountain, D.M., 1995. Nature and composition of the continental crust: a lower crustal perspective, *Rev. Geophys.,* **33**(3), 267–309.

Rudnick, R.L., McDonough, W.F. & O'Connell, R.J., 1998. Thermal structure, thickness and composition of continental lithosphere, *Chem. Geol.,* **145**(3-4), 395–411.

Rychert, C.A. & Shearer, P.M., 2009. A global view of the lithosphere-asthenosphere boundary, *Science,* **324**(5926), 495–498.

Saltus, R.W. & Hudson, T.L., 2007. Regional magnetic anomalies, crustal strength, and the location of the northern Cordilleran fold–and–thrust belt, *Geology,* **35**(6), 567–570.

Sandwell, D.T. & Smith, W.H., 1997. Marine gravity anomaly from Geosat and ERS 1 satellite altimetry, *J. geophys. Res.,* **102**(B5), 10 039–10 054.

Schaeffer, A.J. & Lebedev, S., 2013a. Imaging the North American continent using waveform inversion of global and USArray data, *Earth planet. Sci. Lett.,* **402,** 26–41.

Schaeffer, A.J. & Lebedev, S., 2013b. Global shear speed of the upper mantle and transition zone, *Geophys. J. Int.,* **194,** 417–449.

Scrutton, R.A., 1982. *Passive Continental Margins: A Review of Observations and Mechanisms,* Geodynamic Series, Vol. 6: Dynamics of Passive Margins, The Geological Society of America.

Sharples, W., Moresi, L.N., Jadamec, M.A. & Revote, J., 2015. Styles of rifting and fault spacing in numerical models of crustal extension, *J. geophys. Res.,* **120**(6), 4379–4404.

Shephard, G.E., Dietmar Müller, R. & Seton, M., 2013. The tectonic evolution of the Artic since Pangea breakup: integrating constraints from surface geology and geophysics with mantle structure, *Earth–Sci. Rev.,* **124,** 148–183.

Simmons, N.A., Myers, S.C., Johannesson, G. & Matzel, E., 2012. LLNL-G3Dv3: Global P wave tomography model for improved regional and teleseismic travel time prediction, *J. geophys. Res.,* **117,** B10302.

Smith, L. & Chapman, D.S., 1983. On the thermal effects of regional groundwater flow: 1. Regional scale systems, *J. geophys. Res.,* **88**(B1), 593–608

Spada, M., Bianchi, I., Kissling, E., Piana Agostinetti, A. & Wiemer, S., 2013. Combining controlled–source seismology and receiver function information to derive 3D Moho topography for Italy, *Geophys. J. Int.,* **194,** 1050–1069.

Tesauro, M., Audet, P., Kaban, M.K., Bürgmann, R. & Cloetingh, S., 2012. The effective elastic thickness of the continental lithosphere: comparison between rheological and inverse approaches, *Geochem. Geophys. Geosyst.,* **13**(9).

Torne, M., Fernàndez, M., Vergés, J., Ayala, C., Salas, M.C., Jiménez–Munt, I., Buffett, G.G. & Díaz, J., 2015. Crust and mantle lithospheric structure of the Iberian Peninsula deduced from potential field modeling and thermal analysis, *Tectonophysics,* **663,** 419–433.

Trop, J.M. & Ridgway, K.D., 2007. Mesozoic and Cenozoic tectonic growth of southern Alaska: a sedimentary basin perspective, in *Tectonic Growth of a Collisional Continental Margin: Crustal Evolution of Southern Alaska,* pp. 55–94, eds Ridgway, K.D. Trop, J.M. Glen, J.M.G. & O′Neill, J.M., Geological Society of America Special Paper. **431**.

Tunini, L., Jiménez-Munt, I., Fernandez, M., Vergés, J. & Villasenor, A., 2016. Lithospheric mantle heterogeneities beneath the Zagros Mountains and the Iranian Plateau: a petrological-geophysical study, *Geophys. J. Int.,* **200**(1), 596–614.

Turcotte, D.L. & Schubert, G., 2014. *Geodynamics,* Cambridge Univ. Press.

Veenstra, E., Christensen, D.H., Abers, G.A. & Ferris, A., 2006. Crustal thickness variation in south-central Alaska, *Geology,* **34**(9), 781–784.

Verzhbitsky, V., Savostina, T., Frantzen, E., Little, A., Sokolov, S.D. & Tuchkova, M.I., 2008. Russian Chukchi Sea, *GEOExPro,* **5,** 3.

Waldhauser, F., Kissling, E., Ansorge, J. & Mueller, S., 1998. Three–dimensional interface modelling with two–dimensional seismic data: the Alpine crust–mantle boundary, *Geophys. J. Int.,* **135,** 264–278.

Wang, Y. & Tape, C., 2014. Seismic velocity structure and anisotropy of the Alaska subduction zone based on surface wave tomography, *J. geophys. Res.,* **119**(12), 8845–8865.

Watts, A.B., 2001. *Isostasy and Flexure of the Lithosphere,* Cambridge Univ. Press.

Wessel, P., Smith, W.H.F., Scharroo, R., Luis, J. & Wobbe, F., 2013. Generic mapping tools: improved version released, *EOS, Trans. Am. geophys. Un.,* **94**(45), 409–410.

Worthington, L.L., Van Avendonk, H.J., Gulick, S.P., Christeson, G.L. & Pavlis, T.L., 2012. Crustal structure of the Yakutat terrane and the evolution of subduction and collision in southern Alaska, *J. geophys. Res.,* **117**(B1).